Interlayer RKKY coupling in bulk Rashba semiconductors under topological phase transition

Mahmoud M. Asmar and Wang-Kong Tse

Phys. Rev. B **100**, 014410 — Published 8 July 2019

DOI: 10.1103/PhysRevB.100.014410

Interlayer RKKY Coupling in Bulk Rashba Semiconductors under Topological Phase Transition

Mahmoud M. Asmar and Wang-Kong Tse
Department of Physics and Astronomy, Center for Materials for Information Technology, The University of Alabama, Tuscaloosa, AL 35487, USA
(Dated: June 6, 2019)

The bulk Rashba semiconductors BiTeX (X=I, Cl and Br) with intrinsically enhanced Rashba spin-orbit coupling provide a new platform for investigation of spintronic and magnetic phenomena in materials. We theoretically investigate the interlayer exchange interaction between two ferromagnets deposited on opposite surfaces of a bulk Rashba semiconductor BiTeI in its trivial and topological insulator phases. In the trivial phase BiTeI, we find that for ferromagnets with a magnetization orthogonal to the interface, the exchange coupling is reminiscent of that of a conventional three-dimensional metal. Remarkably, ferromagnets with a magnetization parallel to the interface display a magnetic exchange qualitatively different from that of conventional three-dimensional metal due to the spin-orbit coupling. In this case, the interlayer exchange interaction acquires two periods of oscillations and decays as the inverse of the thickness of the BiTeI layer. For topological BiTeI, the magnetic exchange interaction becomes mediated only by the helical surface states and acts between the one-dimensional spin chains at the edges of the sample. The surface state-mediated interlayer exchange interaction allows for the coupling of ferromagnets with non-collinear magnetization and displays a decay power different from that of trivial BiTeI, allowing the detection of the topological phase transition in this material. Our work provides insights into the magnetic properties of these newly discovered materials and their possible functionalization.

I. INTRODUCTION

The Rashba spin-orbit coupling (SOC) in materials arises from broken spatial inversion symmetry. It has been extensively studied in two-dimensional (2D) electron systems such as heterointerfaces of semiconductors, thin films and surfaces of heavy metals [1–6]. Due to broken inversion symmetry in these systems, electrons experience a perpendicular electric field $\boldsymbol{E}$, which generates a spin-orbit coupling $\boldsymbol{E}\cdot(\boldsymbol{\sigma}\times\boldsymbol{k})$ that depends on the electrons' momentum $\boldsymbol{k}$ and spin $\boldsymbol{\sigma}$. This Rashba effect in a 2D electron gas splits the spin-degenerate parabolic bands into dispersions with opposite spin polarizations [7].

Three-dimensional (3D) materials with *intrinsically* broken inversion symmetry can also exhibit Rashba SOC. Recent theoretical and experimental studies have revealed a giant Rashba splitting in bismuth tellurohalides BiTeX (X=I,Cl and Br) due to the large internal electric field between the constituent layers of these materials [8–13]. These materials became known as bulk Rashba semiconductors. The Rashba semiconductor BiTeI, in particular, has been shown to undergo a pressure-controlled topological phase transition [14–18]. As this material is subjected to an increasing hydrostatic pressure it transitions from a non-topological phase to a strong topological insulator phase, at approximately 3 GPa [14–17], and these two phases are separated by an intermediate Weyl phase [19–21]. Rashba semiconductors have generated much interest as a new material platform for spintronics and controlled topological phenomena [22–26].

Heterostructures composed of magnetic and non-magnetic materials are an important platform that allow controlled information transfer between spins [27, 28]. The key ingredient to this transfer is the effective interaction between the magnetic moments mediated by the conduction electrons of the non-magnetic host material. This effective interaction is known as the Ruderman-Kittel-Kasuya-Yosida (RKKY) or the indirect carrier-mediated exchange interaction [29–31]. The theory of RKKY interaction was initially formulated to address the problem of the interaction between magnetic impurities in the bulk of a metal. Because it is carrier-mediated, RKKY interaction depends on the dimensionality of the host metal and the nature of its low-energy fermionic excitations [32–36]. In 3D conventional metals characterized by a single spin-degenerate parabolic band, the strength of this interaction undergoes oscillations as a function of the impurities' separation r at a period $\lambda_F/2$ given by the Fermi wavelength λ_F, while the envelope of the oscillations decays as r^{-3} [29–31]. The same physical mechanism occurs in a ferromagnet-normal metal-ferromagnet (FM/NM/FM) trilayer structure, with each of the ferromagnetic layers forming a 2D collection of spins at the interface and the metal spacer mediating the indirect exchange interaction. The RKKY theory was generalized in the seminal work by Bruno and Chappert [37] to describe the oscillatory interlayer exchange coupling between the ferromagnetic layers. For a conventional metallic spacer such as Au or Cu, it predicts multiple oscillation periods of the coupling decaying as the inverse square of the spacer thickness, *i.e.* z^{-2} [38]. A review of interlayer exchange coupling in magnetic multilayers can be found in Ref. [39].

The interplay between magnetic and spin-orbit effects provides the basis for a number of wide-ranging phenomena, such as topological phases of matter, magnetic domain walls, Majorana bound states and magnetic

skyrmions [24–26, 40–42]. Hence, the strong and intrinsically generated Rashba SOC in bismuth tellurohalides and their pressure-controlled topological phases promise to provide important insights on the heretofore unexplored interlayer exchange coupling mediated by these materials.

In this paper, we consider the problem of interlayer exchange coupling mediated by conduction electrons in a bulk Rashba semiconductor, in its trivial and topological phases, between ferromagnetic layers. The main ingredient of our theory is the q_z-dependent static spin susceptibility, which we have obtained analytically. The closed-form result of the spin susceptbility facilitates identification of the Fermi surface singularities (Kohn anomalies) and enables us to capture the salient long-range dependence of the interlayer exchange coupling, including the periods of its oscillations and the spatial decay of its envelope. In the non-topological phase, our theory predicts that the interlayer coupling is strongly dependent on the magnetization directions of the ferromagnets. For ferromagnets with magnetization orthogonal to the interface, we find that SOC effects are not prominent and the interlayer exchange coupling behaves as in conventional 3D metals, decaying with the spacer thickness z as z^{-2}. In contrast, SOC effects are found to play an important role when the ferromagnets' magnetization directions are parallel to interface; the dominant contribution of the interlayer exchange coupling is proportional to the Rashba SOC parameter α and decays as z^{-1}. In the topological phase, where the bulk of these materials becomes insulating and the conduction only happens through the surface electrons, the magnetic exchange in the system becomes limited to the magnetic chains at the sample's edges and is mediated by the 2D helical surface states. Unlike the non-topological phase, the interlayer exchange interaction in the topological phase not only couples collinear spins but also non-collinear spins via the Dzyaloshinskii-Moriya (DM) interaction, decaying with the thickness as $z^{-3/2}$. The qualitative differences exhibited by the arrangement of the ferromagnets' magnetization directions highlight the role of the spacer's Rashba SOC and band topology in the magnetic trilayer geometry.

The remainder of this paper is organized as follows. In Sec. II we introduce the low-energy effective model for the Rashba semiconductor BiTeI and describe its Fermi surface and the associated spin textures. We then develop the formalism for the interlayer exchange coupling between two ferromagnets sandwiching the BiTeI layer in Sec III. In Sec. IV, we first employ this formalism to study the interlayer exchange coupling mediated by a 3D electron gas with an anisotropic Fermi surface but without SOC. In Sec. V we turn our attention to the case with BiTeI as the spacer and compare critically the obtained results including Rashba SOC with those obtained without SOC from Sec. IV. The case of two ferromagnets with magnetizations orthogonal to the interface is studied in Sec. V A and the case of two ferromagnets with magnetizations parallel to the interface in Sec. V B. In

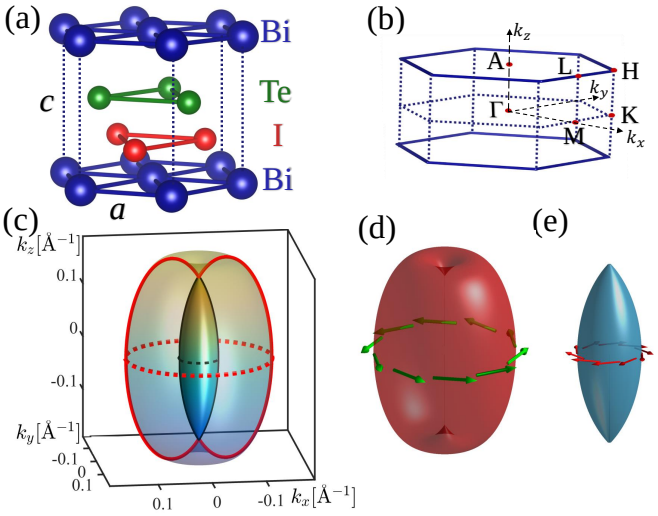

FIG. 1. (a) BiTeI crystal structure. (b) Brillouin zone of BiTeI. (c) Fermi surface of BiTeI centred at the A point for $E_F > 0$. (d) Outer portion of the Fermi surface with negative helicity electrons. (e) Inner portion of the Fermi surface with positive helicity electrons.

Secs. VI and VII we study the interlayer exchange interaction in the topological phase of BiTeI. In Sec. VI the interlayer exchange coupling formalism is adapted to the helical surface states of topological BiTeI, the spin susceptibility of the helical surface states is found and a generic form of the interlayer exchange interaction is derived. In Sec. VII the dependence of the interlayer exchange coupling on the thickness of topological BiTeI is derived. Finally, Secs. VIII and IX provide a discussion of possible experimental realizations and our concluding remarks.

II. BULK RASHBA SEMICONDUCTOR, BiTeI

Bismuth tellurohalides BiTeX (X=I,Cl and Br) generally have a layered lattice structure. In particular, the crystal of BiTeI is composed of a series of asymmetrically stacked triangular layers of Bi, Te and I atoms which leads to an intrinsically broken inversion symmetry along its stacking, c, axis. Fig. 1(a) shows the crystal structure of BiTeI and its corresponding Brillouin zone (BZ) is shown in Fig. 1(b). The asymmetric stacking of the Bi, Te and I layers causes a net polarity along the stacking direction [8–10]. Due to the net polarity along the c-axis, electrons in the a-b plane experience an SOC. The symmetry properties of this SOC are constrained by the space symmetries of the a-b plane. Owing to the threefold symmetry of this plane in BiTeI, the intrinsic 2D SOC in this material inherits this symmetry. At low energies, this symmetry restricts the form of the SOC to $\alpha(\boldsymbol{\sigma} \times \boldsymbol{p}_\parallel)_{\hat{z}}$, where $\boldsymbol{\sigma} = (\sigma_x, \sigma_y, \sigma_z)$ is the vector of Pauli matrix representing spins, $\boldsymbol{p}_\parallel = (p_x, p_y, 0)$ is the in-plane momentum and α is the Rashba SOC strength.

The low-energy electrons of this material are centered in the vicinity of the BZ's hexagonal face center known as the A-point [A= $(0, 0, \pm\pi/c)$] [8–13, 43, 44], and are described by the effective Hamiltonian

$$H_{\rm BiTeI} = Ap_z^2 + B\boldsymbol{p}_\parallel^2 + \alpha(\boldsymbol{\sigma} \times \boldsymbol{p}_\parallel)\hat{z} \ . \tag{1}$$

The material parameters $A \approx 8.04$ eVÅ^2, $B \approx 40.21$ eVÅ^2, [8, 9, 43, 44] $\alpha \approx 3.85$ eVÅ, $c = 6.854$ Å and $a = b = 4.34$ Å have been reported in the literature from photoemission, transport, optical experiments and density functional theory studies [8–13, 43, 44]. Eq. (1) is valid up to a cutoff energy $E_c = 0.2$eV, beyond which the dispersion acquires trigonal warping effects and two additional bands. Since the low-energy Hamiltonian of BiTeI commutes with the helicity operator, $\hat{h} = (\boldsymbol{\sigma} \times \boldsymbol{p}_\parallel)\hat{z}/p_\parallel$, the helicity eigenstates diagonalize $H_{\rm BiTeI}$ and are given by

$$|\boldsymbol{k}, \mu\rangle = \frac{1}{\sqrt{2}} \begin{pmatrix} i \\ \mu e^{i\phi_k} \end{pmatrix} e^{i(\boldsymbol{k}_\parallel \cdot \boldsymbol{r} + k_z z)} \ , \tag{2}$$

where $\boldsymbol{k} = (k_x, k_y, k_z)$, $\phi_k = \tan^{-1}(k_y/k_x)$ is the azimuthal angle of $\boldsymbol{k}_\parallel = (k_x, k_y, 0)$ and $\mu = \pm$ is the helicity of the eigenstate. The corresponding energy eigenvalues are

$$E_{\boldsymbol{k},\mu} = Ak_z^2 + Bk_\parallel^2 + \mu\alpha k_\parallel \ , \tag{3}$$

where $k_\parallel = \sqrt{k_x^2 + k_y^2}$. Stoichiometric BiTeI is an n-doped semiconductor where the Fermi energy is located above the Dirac node that results from the Rashba SOC [8, 9, 43, 45]. As we explain in Fig. 1, the Fermi surface for $E_F > 0$ consists of two segments characterized by states with opposite helicities. The in-plane momenta that span these two parts of the Fermi surface individually can be obtained by solving for $k_\parallel$ from the dispersion $Ak_z^2 + Bk_\parallel^2 + \mu\alpha k_\parallel = E_F$ for a particular value of k_z. The radii k_μ for a given k_z plane for the positive (negative) helicity segment of the Fermi surface is determined as

$$k_\mu = k_F - \mu\frac{\alpha}{2B}, \quad \text{for } k_z \le k_D \tag{4a}$$

$$k_- = \pm k_F + \frac{\alpha}{2B}, \text{ for } |k_z| \ge k_D \ . \tag{4b}$$

where $\pm k_D$, with $k_D = \sqrt{E_F/A}$, specify the locations of the two Dirac points along the k_z axis and $k_F = \sqrt{E_F + \alpha^2/4B - Ak_z^2}/\sqrt{B}$. Additionally, the upper bound on k_z follows from the condition that k_- and hence k_F must be real, leading to

$$|k_z| \le \sqrt{k_D^2 + \frac{\alpha_R^2}{4AB}} \equiv k_m \ . \tag{5}$$

The helicity-resolved segments of the Fermi surface are shown in Fig. 1(c)-(e). Outside the Dirac nodes ($k_D < |k_z| < k_m$), only the negative helicity states exist. Between the Dirac nodes however ($|k_z| < k_D$), states with

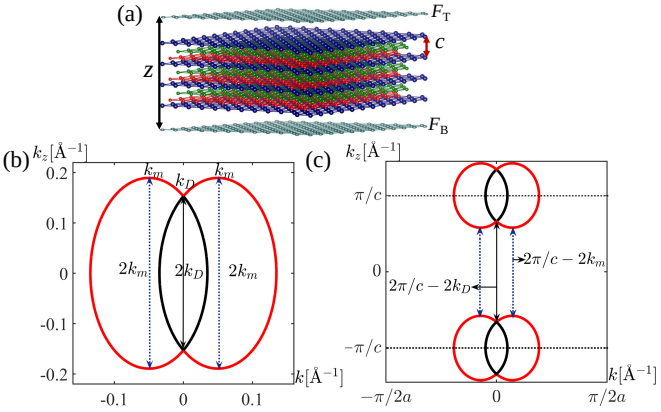

FIG. 2. (a) Atomic configuration of the Ferromagnet-BiTeI-Ferromagnet multilayered system. The top (bottom) ferromagnetic layer is indicated by $F_{\rm T}$ ($F_{\rm B}$), and the distance between $F_{\rm T}$ and $F_{\rm B}$ is $z = (N+1)c$, where c is the thickness of a BiTeI single layer and N is an integer. (b) BiTeI Fermi surface projection centered at the A point. The arrows indicate the critical spanning vectors determined by the Fermi function and the spin textures. (c) BiTeI Fermi surface projection defined in its periodic BZ. The critical spanning vectors resulting from the connection between the extrema of Fermi surfaces at $\pm\pi/c$ are equivalent to those in (b) and result in the same period of oscillation.

oppositive helicities coexist in the inner and outer sections of the Fermi surface. The spin textures associated with the inner ($\mu = +$) and outer ($\mu = -$) portions of the Fermi surface are given by

$$\langle\sigma_x\rangle = \mu \sin\phi_k \ \text{ and } \ \langle\sigma_y\rangle = -\mu\cos\phi_k \ . \tag{6}$$

As displayed in Fig. 1(d)-(e), the two helical branches of Fermi surface are characterized by opposite sense of rotations of the electron spins.

III. FORMALISM OF INTERLAYER EXCHANGE INTERACTION: TRIVIAL PHASE

We employ the RKKY formalism for interlayer exchange coupling in Refs. [37, 38]. Our system consists of two ferromagnets ($F_{\rm T}$ and $F_{\rm B}$) sandwiching BiTeI along its stacking direction, as shown in Fig 2(a). The distance between the ferromagnets is $z = (N+1)c$, where c thickness of a BiTeI unit cell and N is an integer, see Fig. 1(a). The ferromagnetic layer adjacent to BiTeI is assumed to consist of classical spins $\boldsymbol{S}_i$ located at the atomic position $\boldsymbol{R}_i$ of the spacer material BiTeI. The spins $\boldsymbol{S}_i$ of the ferromagnetic layer are coupled to the electron spins of the BiTeI via a contact potential at the interface, $\mathcal{V}_i = J_0\delta(\boldsymbol{r} - \boldsymbol{R}_i)\mathcal{S}\cdot\boldsymbol{S}_i$, where J_0 is the amplitude of the potential and $\mathcal{S}$ is the electron spin operator of the BiTeI spacer. Within these considerations, the

interlayer coupling can be expressed as follows

$$I(z) = -\sum_{a,b=x,y,z} \frac{J_0^2 S_a^{\mathrm{T}} S_b^{\mathrm{B}} c}{2(2\pi)^3 V_0} \int_{-\pi/c}^{\pi/c} dq_z e^{iq_z z} \times \int_{2\mathrm{DBZ}} d^2\boldsymbol{q}_\parallel \chi_{ab}(\boldsymbol{q}_\parallel, q_z) \sum_{\boldsymbol{R}\in F_{\mathrm{T}}} e^{i\boldsymbol{q}_\parallel\cdot\boldsymbol{R}}, \quad (7)$$

where V_0 is the volume of the unit-cell, $S^{(\mathrm{T,B})}_{x,y,z}$ are the spin projections of the top (T) and bottom (B) ferromagnetic layers, and $\chi_{ab}(\boldsymbol{q}_\parallel, q_z)$ is the ab component of the static spin susceptibility tensor. The planar dimensions of the ferromagnetic layers satisfy periodic boundary conditions since they are assumed to be large compared to the interlayer distance. The last sum in Eq. (7) is then nonzero only for $\boldsymbol{q}_\parallel = 0$. Recalling that the area of the projected 2D BZ for BiTeI is $(2\pi)^3 c/(2\pi V_0)$ [where $(2\pi)^3/V_0$ is the volume of the 3D BZ], the interlayer exchange coupling can be written as

$$I_{ab}(z) = -\frac{1}{2}\left(\frac{J_0}{V_0}\right)^2 \frac{S_a^{\mathrm{T}} S_b^{\mathrm{B}} c^2}{2\pi} \int_{-\pi/c}^{\pi/c} dq_z \times e^{iq_z z} \chi_{ab}(\boldsymbol{q}_\parallel = 0, q_z). \quad (8)$$

The components of spin susceptibility, χ_{ab}, for BiTeI consist of intraband and interband contributions. For simplicity, in the sections running up to Sec. V B we omit the $\boldsymbol{q}_\parallel = 0$ argument in χ_{ab} and denote $\chi_{ab}(q_z) \equiv \chi_{ab}(\boldsymbol{q}_\parallel = 0, q_z)$. Since the bands of BiTeI are characterized by their helicity, the spin susceptibility can be written as $\chi_{ab}(q_z) = \sum_{\mu,\nu=\pm} \chi^{\mu\nu}_{ab}(q_z)$ with

$$\chi^{\mu\nu}_{ab}(q_z) = \frac{-\mu_B^2}{(2\pi)^3} \int_{-\pi/c}^{\pi/c} dk_z \int_{2\mathrm{DBZ}} d^2\boldsymbol{k}_\parallel \times \frac{f(E_{\boldsymbol{k},\mu}) - f(E_{\boldsymbol{k}+q_z,\nu})}{E_{\boldsymbol{k},\mu} - E_{\boldsymbol{k}+\boldsymbol{q}_z,\nu} + i\delta} \mathcal{F}^{\mu\nu}_{ab}(\boldsymbol{k}, \boldsymbol{k}+\boldsymbol{q}_z), \quad (9)$$

where $\mu, \nu = \pm$, $f(E_{\boldsymbol{k},\mu})$ is the Fermi function, μ_B is the Bohr magneton, δ is a positive infinitesimal, and $\mathcal{F}^{\mu\nu}_{ab}(\boldsymbol{k}, \boldsymbol{k}+\boldsymbol{q}) = \langle \mu, \boldsymbol{k}|\sigma_a|\boldsymbol{k}+\boldsymbol{q}, \nu\rangle\langle \nu, \boldsymbol{k}+\boldsymbol{q}|\sigma_b|\boldsymbol{k}, \mu\rangle$ is a form factor (see Appendix A). In this work, we consider low temperatures $k_{\mathrm{B}}T \ll E_F$ and take $T = 0$ in Eq. (9).

The oscillatory nature of interlayer RKKY interaction is due to the spatial oscillations of the induced spin density by the localized moments of the ferromagnetic layers and shares the same physical origin as the Kohn anomaly [46]. It stems from the sharpness of the Fermi surface at zero temperature and is measured by the critical spanning vectors (also called calipers). A critical spanning vector is one that connects a pair of extremum points of the Fermi surface along k_z. These critical spanning vectors determine the periods of oscillations as a function of the spacer thickness. Because the thinnest possible spacer is one with a single unit cell, the smallest observable period is twice the unit cell thickness $2c$ corresponding to a critical spanning vector of π/c. If the Fermi surface yields a critical spanning vector that is larger than π/c, a period that is longer than that given directly by the critical spanning vector will be observed instead because the latter cannot be sampled. This effect is known as aliasing and was observed in the interlayer exchange coupling mediated by noble metals, *e.g.*, Fe/Cu, Fe/Cr and Co/Cu [47, 48].

In BiTeI, the largest critical spanning vector defined by its Fermi surface is $2k_m$ [see Eq. (5)] corresponding to the period π/k_m, as shown in Fig. 2(b). The effect of aliasing would manifest in the case when the period resulting from the largest spanning vector is shorter than $2c$. Within our low-energy model for BiTeI, the Fermi energy is bounded from above by the cutoff energy $E_c = 0.2$ eV, and the corresponding k_m is small such that π/k_m exceeds $2c$. Therefore, aliasing does not occur for the critical spanning vectors $2k_m, 2k_D$ calipering the Fermi surface from the *inside*. As shown in Fig. 2(c), the other two critical spanning vectors $2\pi/c - 2k_m, 2\pi/c - 2k_D$ calipering the Fermi surface from the *outside* are equivalent to $2k_m, 2k_D$, respectively. Hence, the limits of integration in Eq. (9) are only determined by the boundaries of the two helical Fermi surfaces through the Fermi functions. To make this explicit, it is useful to define a function $g^{\mu\nu}(k_z)$ that captures the k_z dependence of the helicity content of the bands, with $g^{\mu\nu}(k_z) = \Theta(k_D - k_z)\Theta(k_D + k_z)$ for $\mu = -\nu$ and $\mu = \nu = +$ and $g^{\mu\nu} = 1$ for $\mu = \nu = -$, where Θ is the Heaviside step function. We can then write Eq. (9) as an integral over the entire momentum space constrained by $g^{\mu\nu}(k_z)$,

$$\chi^{\mu\nu}_{ab}(q_z) = \frac{-\mu_B^2}{(2\pi)^3} \int dk_z\, g^{\mu\nu}(k_z) \int d^2\boldsymbol{k}_\parallel \times \frac{f(E_{\boldsymbol{k},\mu}) - f(E_{\boldsymbol{k}+\boldsymbol{q}_z,\nu})}{E_{\boldsymbol{k},\mu} - E_{\boldsymbol{k}+\boldsymbol{q}_z,\nu} + i\delta} \mathcal{F}^{\mu\nu}_{ab}(\boldsymbol{k}, \boldsymbol{k}+\boldsymbol{q}_z), \quad (10)$$

The form factor $\mathcal{F}^{\mu\nu}_{ab}$ is independent of the momentum along z and is given by

$$\begin{aligned}
&\mathcal{F}^{\mu\nu}_{zz} = \frac{1-\mu\nu}{2},\ \mathcal{F}^{\mu\nu}_{xx} = \frac{1-\mu\nu\cos(2\phi_k)}{2}, \\
&\mathcal{F}^{\mu\nu}_{yy} = \frac{1+\mu\nu\cos(2\phi_k)}{2},\ \mathcal{F}^{\mu\nu}_{xy} = \mathcal{F}^{\mu\nu}_{yx} = -\frac{\sin(2\phi_k)}{2}, \\
&\mathcal{F}^{\mu\nu}_{zx} = -\mathcal{F}^{\mu\nu}_{xz} = \frac{\mu-\nu}{2i}\cos(\phi_k), \\
&\mathcal{F}^{\mu\nu}_{zy} = -\mathcal{F}^{\mu\nu}_{yz} = \frac{\mu-\nu}{2i}\sin(\phi_k). \quad (11)
\end{aligned}$$

Upon angular integration, Eq. (10) gives

$$\chi_{ab}(q_z) = C \begin{cases} 2\int_{-k_D}^{k_D} dk_z \sum_{\mu} \mathcal{P} \int_0^{k_\mu} \left(\frac{1}{E_{\boldsymbol{k}+\boldsymbol{q}_z,-\mu,} - E_{\boldsymbol{k},\mu}} - \frac{1}{E_{\boldsymbol{k},\mu} - E_{\boldsymbol{k}-\boldsymbol{q}_z,-\mu}} \right) k_\parallel dk_\parallel, & \text{if } a=b=z \\ \frac{\chi_{zz}(q_z)}{2C} + \int_{-k_m}^{k_m} dk_z \mathcal{P} \int_0^{k_-} \left(\frac{1}{E_{\boldsymbol{k}+\boldsymbol{q}_z,-} - E_{\boldsymbol{k},-}} - \frac{1}{E_{\boldsymbol{k},-} - E_{\boldsymbol{k}-\boldsymbol{q}_z,-}} \right) k_\parallel dk_\parallel & \\ + \int_{-k_D}^{k_D} dk_z \mathcal{P} \int_0^{k_+} \left(\frac{1}{E_{\boldsymbol{k}+\boldsymbol{q}_z,+} - E_{\boldsymbol{k},+}} - \frac{1}{E_{\boldsymbol{k},+} - E_{\boldsymbol{k}-\boldsymbol{q}_z,+}} \right) k_\parallel dk_\parallel, & \text{if } a=b=(x,y) \\ 0, & \text{if } a \neq b, \end{cases} \tag{12}$$

where $C = \pi\mu_B^2/(2\pi)^3$, k_μ is given in Eq. (4), $k_D = \sqrt{E_F/A}$ and k_m is given in Eq. (5) (see Appendix B).

The Rashba SOC in BiTeI is 2D in nature and only couples to in-plane momentum. The spin susceptibility tensor is therefore anisotropic with diagonal components $\chi_{xx}(q_z) = \chi_{yy}(q_z) \neq \chi_{zz}(q_z)$ and vanishing off-diagonal components $\chi_{ab}(q_z)$ $(a \neq b)$. For ferromagnets with spins normal to the interface, the spin susceptibility only has contributions from interband transitions, limiting these contributions to the part of the Fermi surface that hosts both helicities. When the ferromagnets have spins parallel to interface, the spin susceptibility has contributions from both intraband and interband processes and all regions of the Fermi surface become relevant. RKKY mechanism does not contribute to interlayer magnetic exchange when the spins of the ferromagnets are orthogonal to each other due to the vanishing off-diagonal components of $\chi_{ab}(q_z)$. Consequently, the interlayer exchange coupling between the ferromagnetic layers is given by

$$I(z) = -\sum_{a=x,y,z} \frac{S_a^{\mathrm{T}} S_a^{\mathrm{B}}}{2} \left(\frac{J_0}{V_0}\right)^2 \frac{c^2}{2\pi} \int_{-\infty}^{\infty} dq_z e^{iq_z z} \chi_{aa}(q_z). \tag{13}$$

We note that the integration over q_z in the above can be extended to $\pm\infty$, since all critical spanning vectors are much smaller than π/c within the range of Fermi energy $E_F < 0.2$ eV considered in the low-energy effective theory for BiTeI.

Having laid out the formalism for the interlayer exchange coupling and evaluated the spin susceptibility, we first consider the simpler case without SOC in order to establish a reference scenario to which the SOC effects from a BiTeI spacer (Sec. V) will be compared.

IV. SPECIAL CASE: SPIN-DEGENERATE METAL

In this section we consider a 3D spin-degenerate metal with an anisotropic energy dispersion described by the Hamiltonian in Eq. (1) with $\alpha = 0$. The components of the spin susceptibility tensor become equal and Eq. (12) becomes

$$\chi(q_z) = \frac{2\mu_B^2}{(2\pi)^3} \int dk_z \mathcal{P} \int d^2\boldsymbol{k}_\parallel \frac{f(E_{\boldsymbol{k}}) - f(E_{\boldsymbol{k}+\boldsymbol{q}_z})}{E_{\boldsymbol{k}+\boldsymbol{q}_z} - E_{\boldsymbol{k}}}, \tag{14}$$

where the factor of 2 results from spin degeneracy. The integration over $k_\parallel$ and k_z leads to

$$\chi(q_z) = \frac{\mu_B^2}{(2\pi)^2 B} \begin{cases} k_D - \frac{q_z^2 - 4k_D^2}{4q_z} \log\left|\frac{q_z + 2k_D}{q_z - 2k_D}\right| & \\ & \text{for } q_z \neq 0 \\ 2k_D & \text{for } q_z = 0, \end{cases} \tag{15}$$

with $k_D = \sqrt{E_F/A}$. The expression above yields a critical spanning vector $|q_z| = 2k_D$ at which $\partial\chi(q_z)/\partial q_z$ has a logarithmic singularity. This singularity indicates the presence of a Kohn anomaly which gives rise to spatial oscillations of induced spin densities and consequently the RKKY mediated interlayer exchange [46]. In the limit of $q_z = 0$ and a spherical Fermi surface with $A = B = \hbar^2/2m$ and $E_F = \hbar^2 k_F^2/2m$, Eq. (15) recovers the Pauli susceptibility of a non-interacting 3D Fermi gas $\chi(0) = 3n\mu_B^2/(2E_F) \equiv \mu_B^2 \mathcal{D}(E_F)$, where $n = k_F^3/(3\pi^2)$ is the number of electrons per unit volume and $\mathcal{D}(E_F)$ is the density of states [29].

We now evaluate the interlayer exchange coupling Eq. (13) between the ferromagnetic layers. Since the system is spin-degenerate and $\chi(q_z)$ is an even function of q_z, we can write Eq. (13) for ferromagnetic layers with parallel spins as

$$I(z) = -\frac{1}{2}\left(\frac{J_0}{V_0^2}\right)^2 S_a^{\mathrm{T}} S_a^{\mathrm{B}} \frac{c^2}{2\pi} \int_0^{\infty} dq_z \cos(q_z z)\chi(q_z)\ . \tag{16}$$

The dominant contribution to Eq. (16) can be extracted analytically by expanding the integrand near the Kohn anomaly $q_z \in [2k_D - \epsilon, 2k_D + \epsilon]$ (where $\epsilon \ll 2k_D$)

$$I(z) \approx -\frac{S_a^{\mathrm{T}} S_a^{\mathrm{B}}}{(2\pi)^3 B}\left(\frac{\mu_B J_0 c}{V_0}\right)^2 \int_{2k_D-\epsilon}^{2k_D+\epsilon} dq_z \cos(q_z z) \times \left[k_D + \frac{(q_z - 2k_D)}{2}\log|q_z - 2k_D|\right]\ . \tag{17}$$

Changing variable $q' = q_z - 2k_D$ and integrating by parts twice lead to

$$I(z) \approx -\frac{S_a^{\mathrm{T}} S_a^{\mathrm{B}}}{2(2\pi)^3 B}\left(\frac{\mu_B J_0}{V_0}\right)^2 \left(\frac{c}{z}\right)^2 \sin(2k_D z) \times \int_{-\epsilon}^{\epsilon} dq' \left[\frac{\sin(q'z)}{q'}\right]\ . \tag{18}$$

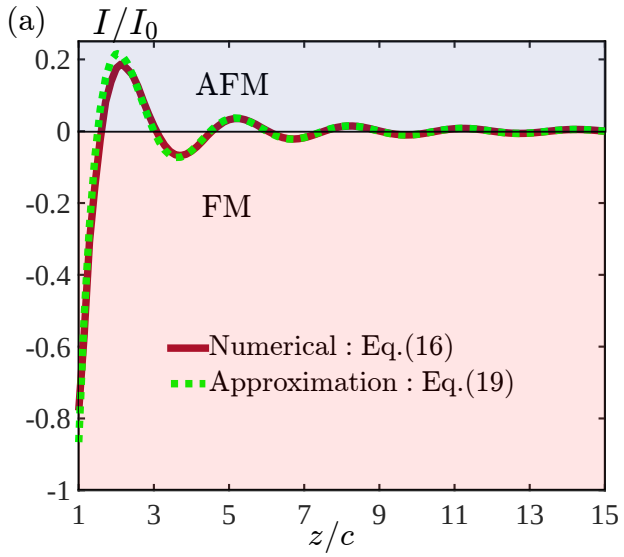

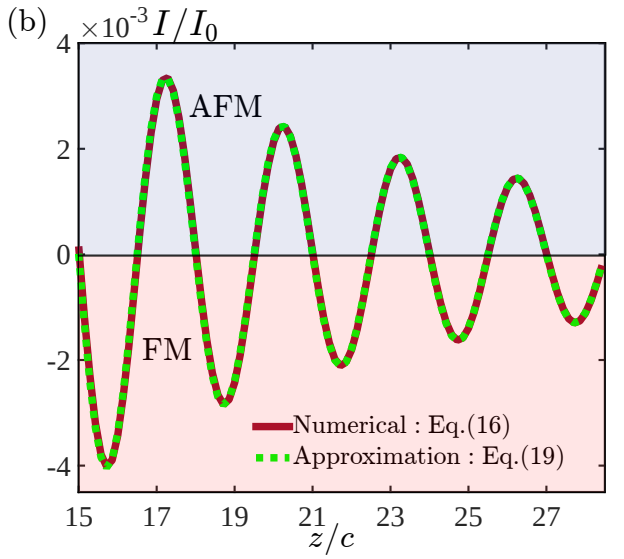

FIG. 3. Exchange coupling between two ferromagnets with parallel spins mediated by a spin-degenerate spacer metal as a function of the ferromagnets' separation z. (a) Shows the z dependence of $I(z)$ for thin spacers. (b) Shows the behaviour of $I(z)$ as function of z for thick spacers. In both (a) and (b) $I(z)$ oscillates with a period π/k_D and this coupling transitions from ferromagnetic (FM) to anti-ferromagnetic (AFM) while decaying as z^{-2}. The Fermi energy for both (a) and (b) is $E_F = 0.18$ eV.

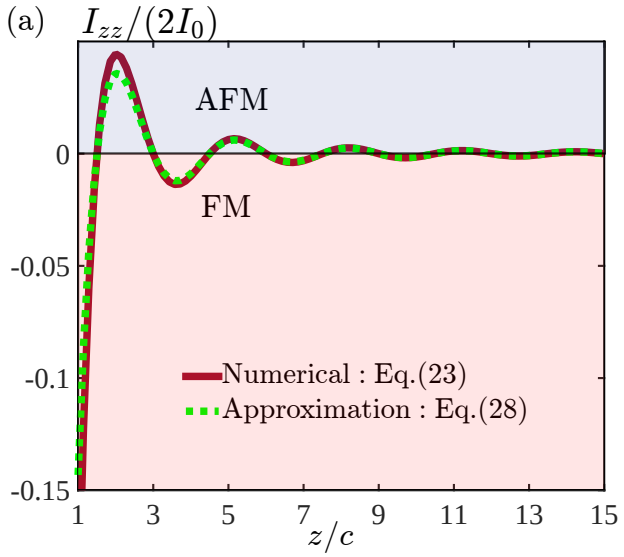

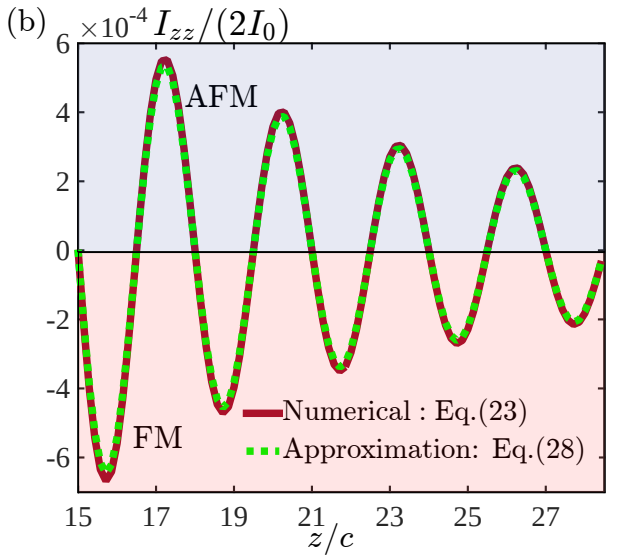

FIG. 4. Thickness dependence of the BiTeI-mediated interlayer magnetic exchange between two z-polarized ferromagnets (Fig. 2) for $E_F = 0.18$ eV. (a) Shows the interlayer exchange coupling for relatively thin samples. (b) Shows the long-range behaviour of the interlayer exchange coupling, *i.e.* relatively thick samples. In both (a) and (b) $I_{zz}(z)$ oscillates with a period π/k_D and this coupling transitions from ferromagnetic (FM) to anti-ferromagnetic (AFM) while decaying as z^{-2}. [Panels (a) and (b) also represent the interband contributions to $I_{xx}(z)$ in Sec. V B].

Since the main contribution of the integral above comes from the vicinity of $q' = 0$, one can extend the limits of this integral to $\pm\infty$, arriving at

$$\frac{I}{I_0} \approx -\left(\frac{c}{z}\right)^2 \sin(2k_D z)\,, \tag{19}$$

where

$$I_0 = \frac{S_a^{\mathrm{T}} S_a^{\mathrm{B}}}{16\pi^2 B}\left(\frac{\mu_B J_0}{V_0}\right)^2 . \tag{20}$$

The analytic result Eq. (19) indicates that the interlayer exchange interaction has a single period of oscillation determined by the critical spanning vector $2k_D$, given by

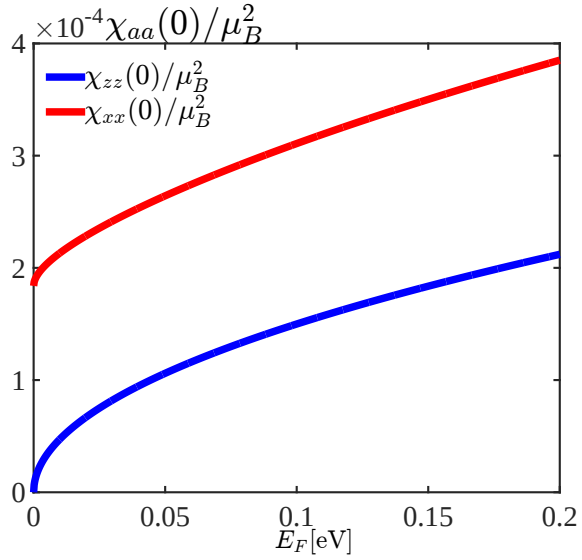

FIG. 5. Long-wavelength behaviour of the spin susceptibility components $\chi_{zz}(0)$ and $\chi_{xx}(0)$ ($\chi_{xx} = \chi_{yy}$) as a function of the Fermi energy. One can notice that $\chi_{xx}(0) > \chi_{zz}(0)$, and that $\chi_{xx}(0)$ is non-vanishing for $E_F = 0$.

π/k_D, and the envelope of the oscillations decay as z^{-2}. In Figs. 3(a) and (b), we plot and compare the interlayer exchange coupling obtained from direct numerical evaluation of Eq. (16) and from Eq. (19). The excellent agreement between the two results confirms that the dominant contribution to the interlayer exchange interaction indeed originates from the critical spanning vector given by the Kohn anomaly of the system, as captured by our approximate analytic result Eq. (19). In the isotropic limit of a spherical Fermi surface with $A = B = \hbar^2/2m$ and $E_F = \hbar^2 k_F^2/2m$, one recovers the well-known result of interlayer exchange interaction obtained by Yafet [49],

$$I(z) \approx -\frac{S_a^{\mathrm{T}} S_a^{\mathrm{B}} m}{8\pi^2\hbar^2}\left(\frac{\mu_B J_0}{V_0}\right)^2\left(\frac{c}{z}\right)^2 \sin(2k_F z)\,. \qquad (21)$$

In this section we have quantified the interlayer exchange coupling between two ferromagnetic layers mediated by a spacer without SOC. In the next two sections, we restore SOC effects and consider BiTeI as the spacer. We will study the interlayer exchange coupling in FM/BiTeI/FM for the two cases when the ferromagnets' spins are aligned perpendicular to the plane and parallel to the plane.

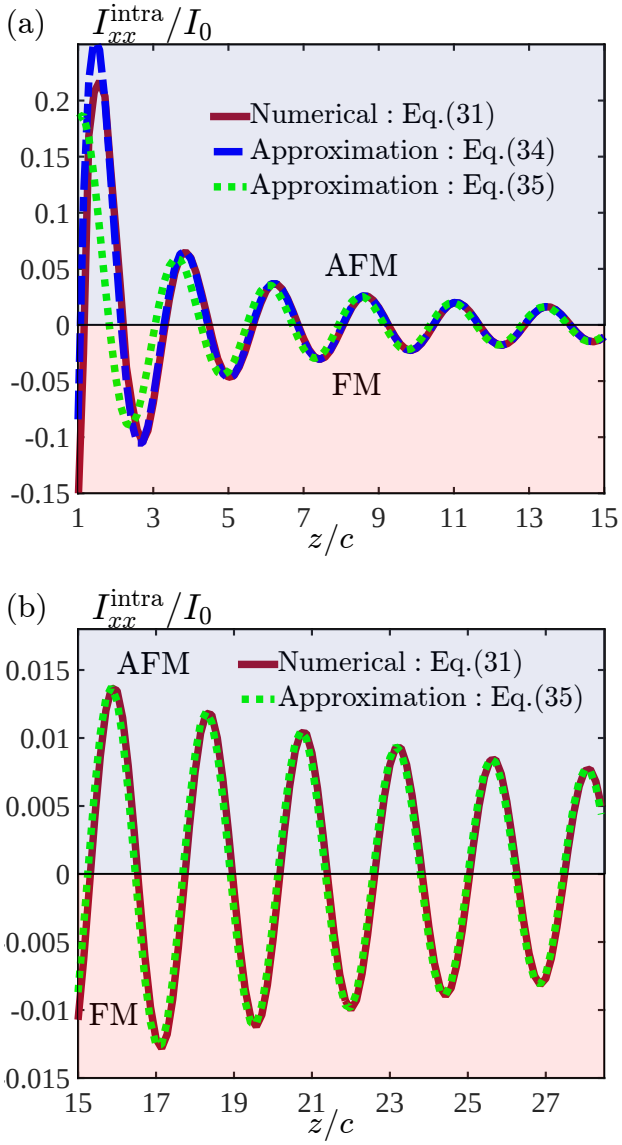

FIG. 6. Intraband contributions to the interlayer exchange coupling $I_{xx}(z)$ for $E_F = 0.18$ eV. Panel (a) shows the dependence for thin BiTeI films. In this case these contributions oscillate with a period π/k_m, the coupling transitions from FM to AFM, and both powers z^{-2} and z^{-1} are necessary to describe its decay. (b) For relatively thick BiTeI samples, the intraband contributions are dominated by a single decay power of z^{-1}, while oscillating with the same period as in (a).

V. INTERLAYER EXCHANGE INTERACTION MEDIATED BY BiTeI

A. Out-of-Plane Magnetization

When the spins of the ferromagnetic layers shown in Fig. 2(a) are in the z-direction, the exchange interaction between F_{T} and F_{B} is mediated by BiTeI electrons that are spin polarized out of the plane and therefore depends on the $\chi_{zz}(q_z)$ component of the spin susceptibility. Since the spin textures of the electronic states in BiTeI are helical and have no out-of-plane components, only interband processes contribute to $\chi_{zz}(q_z)$ and its form factor $\mathcal{F}_{zz}^{\mu\nu} = (1 - \mu\nu)/2$ vanishes for $\mu = \nu$. Since interband transitions require a change in helicity, the region of the Fermi surface that contributes to $\chi_{zz}(q_z)$ is limited to $|k_z| < k_D$, leading to the form of $\chi_{zz}(q_z)$ in

Eq. (12). Integrating $\chi_{zz}(q_z)$ over $k_\parallel$ and k_z leads to

$$\frac{\chi_{zz}(q_z)}{2C} = \frac{2k_D}{B} + \frac{Aq_z}{8}\left[\left(\frac{4k_D^2+q_z^2}{\alpha^2} - \frac{q_z^2-4k_D^2}{ABq_z^2+\alpha^2}\right)\log\left|\frac{2k_D+q_z}{2k_D-q_z}\right| + \left(\frac{4k_D^2+q_z^2}{\alpha^2} + \frac{q_z^2-4k_D^2}{ABq_z^2+\alpha^2}\right) \times \log\left|\frac{q_z(2k_D-q_z)-2\alpha^2/(AB)}{q_z(2k_D+q_z)+2\alpha^2/(AB)}\right|\right] + \frac{Ak_Dq_z^2}{2\alpha^2}\log\left|\frac{q_z^2(q_z^2-4k_D^2)}{[q_z(2k_D+q_z)+2\alpha^2/(AB)][q_z(2k_D-q_z)-2\alpha^2/(AB)]}\right| , \quad (22)$$

where $C = \mu_B^2\pi/(2\pi)^3$. The long-wavelength limit of the spin susceptibility due to z-polarized ferromagnets is $\chi_{zz}(0) = 4Ck_D/B$. This component of the spin susceptibility is known as the van Vleck susceptibility, originating from virtual interband transitions and in this case is identical to the case without SOC [Eq. (15)] [50–54]. Since the spin susceptibility $\chi_{zz}(q_z)$ is an even function of q_z, we can express the interlayer exchange coupling as

$$I_{zz}(z) = -\left(\frac{J_0}{V_0}\right)^2 S_z^{\rm T}S_z^{\rm B}\frac{c^2}{2\pi}\int_0^\infty dq_z\cos(q_zz)\chi_{zz}(q_z) . \quad (23)$$

The spin susceptibility in Eq. (22) reveals the presence of three critical spanning vectors at $|q_z| = 2k_D$, and $|q_z| = k_D \pm \sqrt{k_D^2 - 2\alpha^2/(AB)} = k_n^\pm$. When $|q_z|$ takes the value of a critical spanning vector, $\partial\chi_{zz}(q_z)/\partial q_z$ has a logarithmic divergence, *i.e.* Kohn anomaly [46]. The contributions of the Kohn anomalies to interlayer exchange interaction depend on the Fermi energy of the system. The anomalies associated with the vectors $k_n^\pm$ contribute to the interlayer exchange interaction only when $E_F > 2\alpha^2/B$, while $2k_D$ contributes for any value of the Fermi energy. We numerically evaluate the integral in Eq. (31), and analytically determine the dominant behavior of $I_{zz}(z)$ by considering the contributions $I_{zz}^{(1)}(z)$ and $I_{zz}^{(2,3)}(z)$ of the Kohn anomalies associated with $2k_D$ and $k_n^\pm$, respectively. The latter is done by integration over a small interval enclosing these anomalies.

In the vicinity of $q_z \approx 2k_D$, the interlayer exchange interaction is

$$I_{zz}^{(1)}(z) \approx -\frac{S_z^{\rm T}S_z^{\rm B}}{(2\pi)^3}\left(\frac{\mu_BJ_0c}{V_0}\right)^2\int_{2k_D-\epsilon}^{2k_D+\epsilon}dq_z\left[\mathcal{C} + \frac{Ak_D^2(q_z-2k_D)}{4ABk_D^2+\alpha^2}\log|q_z-2k_D|\right]\cos(q_zz) . \quad (24)$$

Here $\epsilon \ll 2k_D$, and $\mathcal{C}$ is a constant. Following similar steps that lead to Eq. (19), we obtain the contribution of $2k_D$ to the interlayer exchange interaction

$$I_{zz}^{(1)}(z) \approx -2I_0\left(\frac{Ak_D^2}{4ABk_D^2+\alpha^2}\right)\left(\frac{c}{z}\right)^2\sin(2k_Dz) , \quad (25)$$

where I_0 is given in Eq. (20). In the vicinity of $k_n^\pm$ the interlayer exchange coupling $I_{zz}^{(2,3)}(z)$, where the superscript 2 (3) denotes the contribution of k_n^+ (k_n^-), takes the form

$$I_{zz}^{(2,3)}(z) \approx -\frac{S_z^{\rm T}S_z^{\rm B}}{(2\pi)^3}\left(\frac{\mu_BJ_0c}{V_0}\right)^2\int_{k_n^\pm-\epsilon}^{k_n^\pm+\epsilon}dq_z\left[\mathcal{C}_\pm + \frac{k_n^\pm-k_D}{B(2k_D+k_n^\pm)}\log|q_z-k_n^\pm|\right]\cos(q_zz) , \quad (26)$$

where $\mathcal{C}_\pm$ is a constant. Following a similar procedure as in the case of k_D we obtain the contributions of $k_n^\pm$ to the interlayer exchange interaction

$$I_{zz}^{(2,3)}(z) \approx -2I_0\left[\frac{k_n^\pm-k_D}{B(2k_D+k_n^\pm)}\right]\left(\frac{c}{z}\right)^2\sin(k_n^\pm z) . \quad (27)$$

Hence, the total exchange interaction $I_{zz}(z) = \sum_{i=1}^3 I_{zz}^{(i)}(z)$ is given by

$$I_{zz}(z) \approx -2I_0\left[\left(\frac{Ak_D^2}{4ABk_D^2+\alpha^2}\right)\left(\frac{c}{z}\right)^2\sin(2k_Dz) + \Theta\left(E_F-\frac{2\alpha^2}{B}\right)\sum_{j=\pm}\frac{k_n^j-k_D}{B(2k_D+k_n^j)}\left(\frac{c}{z}\right)^2\sin(k_n^jz)\right] . \quad (28)$$

Within our low-energy theory for BiTeI, the maximum Fermi energy given by the energy cutoff of 0.2 eV is smaller than the value of $2\alpha^2/B = 0.74$ eV, and thus the second term in Eq. (28) does not contribute. Hence, as shown in Figs. 4(a) and (b), the BiTeI-mediated exchange between two z-polarized magnetic layers only has a single period of oscillation determined by π/k_D. In addition to the oscillatory behavior of the interlayer exchange coupling we notice that $I_{zz}(z)$ decays as z^{-2}. This behavior is reminiscent of conventional 3D metallic spacers. Moreover, in the limit of $\alpha = 0$, $k_n^+ = 2k_D$ and $k_n^- = 0$, we recover the interlayer exchange coupling in the absence of SOC in Eq. (19).

In this section we have seen that the interlayer exchange coupling between two z-polarized ferromagnets mediated by BiTeI displays a behavior similar to that of a conventional 3D metal and that the SOC coupling only renormalizes the amplitude of this coupling by a factor $2Ak_D^2/(4ABk_D^2+\alpha^2)$. In the next section, we will show that the SOC has a dramatic effect on the interlayer exchange coupling between two ferromagnets with spin polarization parallel to the interface with BITeI.

B. In-Plane Magnetization

In order to study the interlayer exchange coupling between two ferromagnets with spins parallel to the interface with BiTeI [Fig. 2(a)], we consider both ferromagnets [$F_{\rm T}$ and $F_{\rm B}$ in Fig. 2(a)] to have spins aligned in the x-direction without loss of generality. The interaction between the ferromagnets $F_{\rm T}$ and $F_{\rm B}$ depends on the element $\chi_{xx}(q_z)$ of the spin susceptibility tensor in Eq. (12), which contains contributions from both interband and intraband transitions. Hence, unlike the case of the z-polarized ferromagnets, the spin susceptibility in this case has contributions from all regions of the Fermi surface as shown in Eq. (12).

The interband contribution of $\chi_{xx}(q_z)$ is given by $\chi_{zz}(q_z)/2$, and its contributions to the interlayer exchange coupling is $I_{zz}(z)/2$, where $I_{zz}(z)$ is given in Eq. (28). On the other hand, the intraband component of the spin susceptibility, $\chi_{xx}(q_z)$ in Eq. (12), can be written as

$$\frac{\chi^{\rm intra}_{xx}(q_z)}{C} = \int_{-k_D}^{k_D} dk_z \sum_{\mu=\pm} \mathcal{P} \int_0^{k_\mu} \left[\frac{2}{A(q_z^2-4k_z^2)}\right] k dk + 2\int_{k_D}^{k_m} dk_z \sum_{\mu=\pm} \mathcal{P} \int_0^{-\mu k_\mu} \left[\frac{2}{A(q_z^2-4k_z^2)}\right] k dk \,, \tag{29}$$

where $k_D = \sqrt{E_F/A}$, and k_μ, k_m are given in Eq. (4) and Eq. (5), respectively. Integrating Eq. (29) over $k_\parallel$ and k_z gives

$$\chi^{\rm intra}_{xx}(q_z) = \frac{C}{B}\begin{cases} k_m - \dfrac{(q_z^2-4k_m^2)}{4q_z}\log\left|\dfrac{q_z+2k_m}{q_z-2k_m}\right| + \dfrac{\alpha^2}{4ABq_z}\log\left|\dfrac{q_z+2k_m}{q_z-2k_m}\right|, & \text{if } q_z \neq 0 \\ 2k_m + \dfrac{\alpha^2}{4ABk_m}, & \text{if } q_z = 0. \end{cases} \tag{30}$$

Before proceeding to the interlayer exchange interaction between the x-polarized ferromagnets, we find the long-wavelength limit of the spin susceptibility $\chi_{xx}(0) = \chi_{zz}(0)/2 + \chi^{\rm intra}_{xx}(0) = C[2k_m + 2k_D + \alpha^2/(4ABk_m)]/B$, where $C = \mu_B^2\pi/(2\pi)^3$. The latter is the sum of the van Vleck and Pauli susceptibilities [50–53]. Moreover, we notice that $\chi_{xx}(0) > \chi_{zz}(0)$ for $E_F \geq 0$ (see Fig. 5) and therefore electron spins in BiTeI are more easily polarized in response to a uniform in-plane magnetic field than an out-of-plane field.

The intraband contribution to the interlayer exchange interaction is

$$I^{\rm intra}_{xx}(z) = -\left(\frac{J_0}{V_0}\right)^2 S_x^{\rm T} S_x^{\rm B} \frac{c^2}{2\pi}\int_0^\infty dq_z \times \cos(q_z z)\chi^{\rm intra}_{xx}(q_z)\,, \tag{31}$$

and the total interlayer exchange interaction is given by

$$I_{xx}(z) = I^{\rm intra}_{xx}(z) + \left.\frac{I_{zz}(z)}{2}\right|_{S_z^{(\rm T,B)}\to S_x^{(\rm T,B)}}\,, \tag{32}$$

where $I_{zz}(z)$ is given in Eq. (28).

The intraband component of $\chi_{xx}(q_z)$ Eq. (30) reveals the presence of a critical spanning vector that leads to a Kohn anomaly at $|q_z| = 2k_m$. The contribution of this anomaly to the exchange coupling is found by integrating around a small interval containing it, such that for $|q_z| \approx 2k_m$,

$$I^{\rm intra}_{xx}(z) \approx -\frac{S_x^{\rm T}S_x^{\rm B}}{16\pi^3 B}\left(\frac{\mu_B J_0 c}{V_0}\right)^2 \int_{2k_m-\epsilon}^{2k_m+\epsilon} dq_z \Big[k_m + \frac{(q_z-2k_m)}{2}\log|q_z-2k_m| - \frac{\alpha^2}{4ABk_m}\log|q_z-2k_m|\Big]\cos(q_z z)\,. \tag{33}$$

Following similar steps as before,

$$I^{\rm intra}_{xx}(z) \approx -\frac{I_0}{2}\left[\left(\frac{c}{z}\right)^2 \sin(2k_m z) + \frac{\alpha^2 c}{4ABk_m}\left(\frac{c}{z}\right)\cos(2k_m z)\right]\,. \tag{34}$$

The numerical and analytical evaluations of intraband component of $I(z)$ are shown in Figs. 6(a) and (b). We find that this part of the interlayer exchange interaction oscillates with a period π/k_m. For thin films of BiTeI [Fig. 6(a)], both decay powers [z^{-1} and z^{-2} in Eq. (34)] are essential for $I^{\rm intra}_{xx}(z)$. However, for relatively thick samples of BiTeI [Figs. 6(a) and (b)], *i.e.* $z \approx 5c$, the interlayer exchange interaction is solely determined by the spin-orbit dependent part of $I^{\rm intra}_{xx}(z)$, *i.e*,

$$I^{\rm intra}_{xx}(z) \approx -\frac{I_0}{2}\left[\frac{\alpha^2 c}{4ABk_m}\left(\frac{c}{z}\right)\cos(2k_m z)\right]\,, \tag{35}$$

where the decay power law z^{-1} is sufficient to describe $I^{\rm intra}_{xx}(z)$, as shown in Fig. 6.

Combining the interband and intraband contributions as in Eq. (32), the total exchange between these ferromagnets is given by

$$I_{xx}(z) \approx -\frac{I_0}{2}\left\{\left(\frac{c}{z}\right)^2\left[\sin(2k_m z)+\frac{2ABk_D^2\sin(2k_D z)}{4ABk_D^2+\alpha^2}+\Theta\left(E_F-\frac{2\alpha^2}{B}\right)\sum_{j=\pm}\frac{2(k_n^j-k_D)\sin(k_n^j z)}{(2k_D+k_n^j)}\right]+\left(\frac{c}{z}\right)\frac{\alpha^2 c}{4ABk_m}\cos(2k_m z)\right\}. \quad (36)$$

Here we notice that the two different periods of oscillation result from the interband and intraband contributions to the magnetic exchange interaction. In the limit $\alpha = 0$, $k_n^+ = 2k_c$ and $k_n^- = 0$, one recovers the interlayer exchange coupling in the absence of SOC in Eq. (19).

The interlayer exchange coupling $I_{xx}(z)$ displays four periods of oscillation for $E_F > 2\alpha^2/B$. However, for the low-energy electrons in BiTeI the Fermi energy $E_F < 2\alpha^2/B$ restricts the periods to oscillation to π/k_D and π/k_m.

The presence of a SOC in BiTeI makes the interlayer exchange coupling $I_{xx}(z)$ mediated by this material, Eq. (36), qualitatively different from that of a conventional 3D metal, Eq. (19). These differences are reflected in the experimentally relevant characteristics of this exchange, *i.e.* its oscillation periods and its dependence on the spacer thickness. Whereas the interlayer exchange interaction mediated by a conventional 3D metal has a single oscillatory period and decays as z^{-2}, the interlayer exchange coupling $I_{xx}(z)$ mediated by BiTeI has two periods of oscillation and more strikingly it decays as the inverse the spacer thickness z^{-1}.

A close look at $I_{xx}(z)$, Fig. 7(a), shows that the intraband contribution of $I_{xx}(z)$ is dominant due to its peculiar dependence on z, Eq. (35). Hence, the interband contribution to the interlayer exchange coupling can only be discerned for small BiTeI thickness, $z < 5c$. Moreover, for relatively large thicknesses of BiTeI, $z > 5c$ [Figs. 7(a) and (b)], the interlayer exchange coupling is uniquely determined by the term proportional to the SOC coupling that decays as z^{-1} in Eq. (35). Consequently, unlike the case in a conventional 3D metal, the exchange coupling displays an intriguing dependence on the thickness of the BiTeI decaying as z^{-1}, which is reminiscent of the coupling between two magnetic chains mediated by a 2D conventional metal [55, 56]. We attribute this unusual dependence to the 2D nature of the Rashba SOC coupling in BiTeI.

VI. FORMALISM OF INTERLAYER EXCHANGE INTERACTION: TOPOLOGICAL PHASE

BiTeI has been theoretically predicted to undergo a topological phase transition under moderate hydrostatic pressure [14–17]. Subjecting this material to an increasing pressure leads to its transition from its trivial phase to a strong topological insulator phase at approximately 3 GPa [14–17]. These two topologically distinct phases are separated by Weyl semi-metallic phase [19–21]. Experimentally, transport measurements suggest that the topological phase transition happens at the theoretically expected value [18], 3 GPa, while optical experiments suggest that this topological phase transition happens at 9 GPa [15, 17]. In the following two sections, we analyze the interlayer exchange interaction between two ferromagnets mediated by BiTeI in its topological insulator phase and show that it exhibits important differences compared to that in the trivial phase.

In the previous sections we have shown that the interlayer exchange interaction mediated by BiTeI in its trivial phase is dependent on the spin orientation of the magnetic layers [Fig 2(a)] and it only couples collinear spins. The transition of BiTeI from its trivial to its topological insulator phase crucially changes the nature of the magnetic exchange in the system. In its topological phase, BiTeI becomes insulating in the bulk and conducting only through its surfaces. The exchange interaction between magnetic impurities mediated by topological insulator surface states was previously studied [57–65]. In our case, the exchange interaction couples not only two magnetic impurities but two one-dimensional chains of spins at the top and bottom edges of the sample, mediated by the helical electrons residing on the side surfaces. Fig. 8(a) shows our setup with the side surfaces of the rectangular BiTeI sample indicated by S_i, $i = 1, 2, 3, 4$.

In order to study the properties of the interlayer exchange interaction of topological BiTeI we assume that the surface states present on the surfaces S_i are helical and satisfy [24–26, 66–69]

$$H_{\mathrm{S}_i}(\boldsymbol{p}_\parallel) = \hbar v_F(\boldsymbol{\sigma}\times\boldsymbol{p}_\parallel)_{\hat{n}_i}\,, \quad (37)$$

where $\hat{n}_i$ is the normal to the surface S_i, and v_F is the Fermi velocity of the surface states. Adapting Eq. (7) to describe the 2D metallic states that mediate the exchange interaction between two magnetic chains, Fig. 8(b), one arrives at

$$I^i(z) = -\sum_{a,b=x,y,z}\frac{J_0^2 S_a^{\mathrm{T}} S_b^{\mathrm{B}} c}{2(2\pi)^2 A_0}\int_{-\pi/c}^{\pi/c} dq_z e^{iq_z z} \times \int_{1\mathrm{DBZ}} dq_j \chi_{ab}^i(q_j,q_z)\sum_{j\in F_{\mathrm{T}}} e^{iq_j j}\,, \quad (38)$$

here, $i = (1, 2, 3, 4)$ is the surface index [Fig. 8(a)], S_a^{T} (S_b^{B}) is the spin of the top (bottom) magnetic layer, $j = x$ or y depending on the surface S_i, $\chi_{ab}^i(q_j, q_z)$ is the ab component of the spin-susceptibility for a given surface S_i, and A_0 is the area of the 2D BZ enclosing the surface

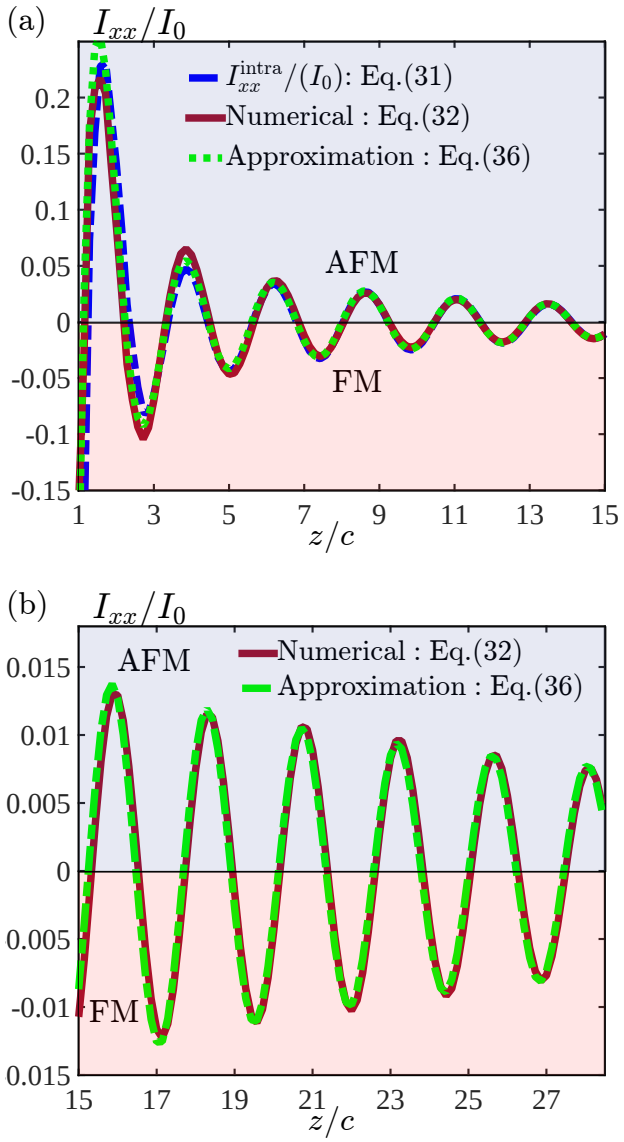

FIG. 7. Thickness dependence of the interlayer exchange coupling between two ferromagnets with spins parallel to the interface (Fig. 2) with $E_F = 0.18$ eV. Panel (a) shows this dependence of $I_{xx}(z)$ for relatively thin samples of BiTeI. In this case $I_{xx}(z)$ oscillates between FM and AFM couplings with two periods, π/k_m and π/k_D. Additionally, the intraband and interband contributions to the coupling can be discerned in this regime since the coupling decays as z^{-1} and z^{-2}, respectively. (b) For relatively thick films of BiTeI, the coupling is dominated by the intraband contributions. It oscillates with a period π/k_m and decays as z^{-1}.

states. It is convenient to analyze the interlayer exchange coupling in Eq. (38) in the set of local coordinates of each surface that transforms the Hamiltonian in Eq. (37) to $H(\boldsymbol{p}_\parallel) = \hbar v_F(\boldsymbol{\sigma} \times \boldsymbol{p}_\parallel)\hat{z}$ for all surfaces. The advantage of this transformation is that the susceptibility components $\chi^i_{ab} = \chi^j_{ab}$ for $i \neq j$. This transformation is achieved by making the local z-axis normal to each surface and

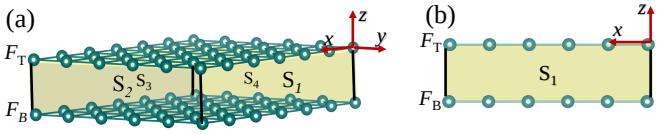

FIG. 8. Schematic representation of (a) magnetic layers sandwiching topological BiTeI. The surface states at $S_{i=1,2,3,4}$ mediate the exchange between the magnetic chains at the edges of the sample as shown in (b). The coordinate axes indicate the global coordinate frame of the system.

the local y-axis pointing to the global z-direction. This also requires the transformation of the magnetic layers' spins $S^{(\rm T,B)}_{a,b}$ in the global coordinates to $\mathcal{S}^{(\rm T,B)}_{c,d}$ in the local coordinates as indicated in Table I and the corresponding transformation of the susceptibility components $\chi^i_{ab} \to \chi_{cd}$. In the local coordinate frame, the interlayer exchange coupling associated with each surface is given by

$$I^i(y) = -\sum_{a,b=x,y,z} \mathrm{sgn}(\mathcal{S}^{i,\rm T}_c \mathcal{S}^{i,\rm B}_d) \frac{J_0^2 S^{\rm T}_a S^{\rm B}_b c}{2(2\pi)^2 A_0} \int_{-\pi/c}^{\pi/c} dq_y e^{iq_y y} \times \int_{\rm 1DBZ} dq_x \chi_{cd}(q_x, q_y) \sum_{x \in F_{\rm T}} e^{iq_x x}\,, \tag{39}$$

here, $\mathcal{S}^{i,(\rm T,B)}_{c,d}$ are the locally transformed spins of the top and bottom magnetic layers, corresponding to $S^{(\rm T,B)}_{a,b}$ in the global coordinates, $\chi_{cd}(q_y)$ is the susceptibility component in local coordinates corresponding to χ^i_{ab} in global coordinates. The transformation of the spins and the spin susceptibility indices between global and local coordinates is given in Table I. The local x-dimensions of

Global Spins	Surface	Local Spins
(S_x, S_y, S_z)	1	$(-\mathcal{S}^1_x, \mathcal{S}^1_z, \mathcal{S}^1_y)$
(S_x, S_y, S_z)	2	$(\mathcal{S}^2_z, \mathcal{S}^2_x, \mathcal{S}^2_y)$
(S_x, S_y, S_z)	3	$(\mathcal{S}^3_x, -\mathcal{S}^3_z, \mathcal{S}^3_y)$
(S_x, S_y, S_z)	4	$(-\mathcal{S}^4_z, -\mathcal{S}^4_x, \mathcal{S}^4_y)$

TABLE I. Transformation of the global spins into the local coordinate system of the surfaces $S_{(1,2,3,4)}$ in Fig. 8. The indices of the global susceptibility transform as the indices of the global spins.

the ferromagnetic layers satisfy periodic boundary conditions since they are assumed to be large compared to the interlayer distance. The last sum in Eq. (39) is then nonzero only for $q_x = 0$. Recalling that the length of the projected 1D BZ of BiTeI is $(2\pi)^2 c/(2\pi A_0)$ [where $(2\pi)^2/A_0$ is the area of the 2D BZ containing the surface states], the interlayer exchange coupling can be written as

$$I^i_{ab}(y) = -\frac{\mathrm{sgn}(\mathcal{S}^{i,\rm T}_c \mathcal{S}^{i,\rm B}_d)}{2} \left(\frac{J_0}{A_0}\right)^2 \frac{S^{\rm T}_a S^{\rm B}_b c^2}{2\pi} \int_{-\pi/c}^{\pi/c} dq_y \times e^{iq_y y} \chi_{cd}(q_x = 0, q_y). \tag{40}$$

The components of spin susceptibility, χ_{cd}, for a helical system described by $H = \hbar v_F(\boldsymbol{\sigma}\times\boldsymbol{p}_\parallel)_{\hat{z}}$ consist of helicity-preserving and helicity-mixing contributions. For simplicity, hereafter we omit the $q_x = 0$ argument in χ_{cd} and denote $\chi_{cd}(q_y) \equiv \chi_{cd}(q_x = 0, q_y)$. Since the surface states are characterized by their helicity, the spin susceptibility can be written as $\chi_{cd}(q_y) = \sum_{\mu,\nu=\pm}\chi^{\mu\nu}_{cd}(q_y)$ with

$$\chi^{\mu\nu}_{cd}(q_y) = \frac{-\mu_B^2}{(2\pi)^2}\int_{-\pi/c}^{\pi/c} dk_y \int_{1\text{DBZ}} dk_x \times \frac{f(E_{\boldsymbol{k}_\parallel,\mu}) - f(E_{\boldsymbol{k}_\parallel+\boldsymbol{q}_y,\nu})}{E_{\boldsymbol{k}_\parallel,\mu} - E_{\boldsymbol{k}_\parallel+\boldsymbol{q}_y,\nu} + i\delta}\mathcal{F}^{\mu\nu}_{cd}(\boldsymbol{k}_\parallel, \boldsymbol{k}_\parallel + \boldsymbol{q}_y), \tag{41}$$

where $\mu,\nu = \pm$ are the helicities of the surface states, $f(E_{\boldsymbol{k}_\parallel,\mu})$ is the Fermi function, $\mathcal{F}^{\mu\nu}_{cd}(\boldsymbol{k}_\parallel, \boldsymbol{k}_\parallel + \boldsymbol{q}_\parallel)$ is the form factor defined in Eq. (9) with the state $|\boldsymbol{k}_\parallel, \mu\rangle = (-i, \mu e^{-i\phi_k})^\dagger e^{i\boldsymbol{k}_\parallel\cdot\boldsymbol{r}}/\sqrt{2}$. By considering that the largest critical spanning vector $2k_F = 2E_c/(\hbar v_F)$, where $E_c \approx 0.2$eV is the cutoff energy of the low-energy theory of the surface states [70], one obtains a period of oscillation that is larger than $2c$, thus, the limits of the integral in Eq. (41) will be restricted only by the Fermi functions, *i.e.*,

$$\chi^{\mu\nu}_{cd}(q_y) = \frac{-\mu_B^2}{(2\pi)^2}\int dk_y \int dk_x \times \frac{f(E_{\boldsymbol{k}_\parallel,\mu}) - f(E_{\boldsymbol{k}_\parallel+\boldsymbol{q}_y,\nu})}{E_{\boldsymbol{k}_\parallel,\mu} - E_{\boldsymbol{k}_\parallel+\boldsymbol{q}_y,\nu} + i\delta}\mathcal{F}^{\mu\nu}_{cd}(\boldsymbol{k}_\parallel, \boldsymbol{k}_\parallel + \boldsymbol{q}_y). \tag{42}$$

In general, for a 2D electron system described by the Hamiltonian $H = \hbar v_F(\boldsymbol{\sigma}\times\boldsymbol{p}_\parallel)_{\hat{z}}$ we evaluated the spin susceptibility tensor components (see Appendix A)

$$\chi_{cd}(\boldsymbol{q}_\parallel) = \frac{-\mu_B^2}{(2\pi)^2}\sum_{\mu,\nu=\pm}\int d^2\boldsymbol{k}_\parallel \times \frac{f(E_{\boldsymbol{k}_\parallel,\mu}) - f(E_{\boldsymbol{k}_\parallel+\boldsymbol{q}_\parallel,\nu})}{E_{\boldsymbol{k}_\parallel,\mu} - E_{\boldsymbol{k}_\parallel+\boldsymbol{q}_\parallel,\nu} + i\delta}\mathcal{F}^{\mu\nu}_{cd}(\boldsymbol{k}_\parallel, \boldsymbol{k}_\parallel + \boldsymbol{q}_\parallel), \tag{43}$$

and find that [71]

$$\chi(\boldsymbol{q}_\parallel) = \begin{pmatrix} g_1(x)\cos^2(\phi_q) & \frac{g_1(x)}{2}\sin(2\phi_q) & g_2(x)\cos(\phi_q) \\ \frac{g_1(x)}{2}\sin(2\phi_q) & g_1(x)\sin^2(\phi_q) & g_2(x)\sin(\phi_q) \\ g_2^*(x)\cos(\phi_q) & g_2^*(x)\sin(\phi_q) & g_3(x) \end{pmatrix} \tag{44}$$

where $\phi_q = \tan^{-1}(q_x/q_y)$, $x = 2k_F/q_\parallel$, $q_\parallel = \sqrt{q_x^2+q_y^2}$, k_F is the Fermi momentum, and

$$\begin{aligned} g_1(x) &= \frac{-\mu_B^2}{4\pi\hbar v_F}\text{Re}\left[\sqrt{1-x^2} + \frac{q}{2}\sin^{-1}\left(\sqrt{1-x^2}\right)\right], \\ g_2(x) &= \frac{-i\mu_B^2 q}{8\pi\hbar v_F}\left[1 - \frac{1}{2}\text{Re}\left(\sqrt{1-x^2}\right)\right], \\ g_3(x) &= \frac{-\mu_B^2}{2\pi\hbar v_F}\left\{k_F + \frac{q}{2}\text{Re}\left[\sin^{-1}\left(\sqrt{1-x^2}\right)\right]\right\}. \end{aligned} \tag{45}$$

In the literature there has been a disagreement on the forms of the functions $g_{1,2,3}(x)$ [57, 58]. In order to find these functions we derived the renormalized susceptibility, which required the substraction of intrinsic susceptibility (the susceptibility at $E_F = 0$) at $\boldsymbol{q}_\parallel = 0$, $\chi^{\text{intrinsic}}_{cd}(0)$, from the total susceptibility $\chi_{cd}(\boldsymbol{q}_\parallel)$. This method is consistent with Refs. [72] and [73] and leads to identical results for the polarization function therein. Taking $q_x = 0$, $\phi_q = \pm\pi/2$ [+ (−) for positive (negative) values of q_y], the susceptibility tensor reduces to

$$\chi(q_y) = \begin{pmatrix} 0 & 0 & 0 \\ 0 & g_1(x) & \text{sgn}(q_y)g_2(x) \\ 0 & \text{sgn}(q_y)g_2^*(x) & g_3(x) \end{pmatrix}, \tag{46}$$

where $x = 2k_F/q_y$ in this case. Since the elements $\chi_{cd}(q_y) = 0$ for $(c,d) = \{(x,x),(x,y),(x,z),(y,x),(z,x)\}$, their associated interlayer exchange coupling is zero. With the remaining non-vanishing susceptibility elements we find that the interlayer exchange coupling for the different surfaces, when expressed in the global coordinates of the system as indicated in Fig. 8, is given by

$$I^i(z) = AS_z^{\text{T}}S_z^{\text{B}} + BS^{\text{T}}_{|\hat{n}_i|}S^{\text{B}}_{|\hat{n}_i|} + D(\boldsymbol{S}^{\text{T}}\times\boldsymbol{S}^{\text{B}})_{\hat{z}\times\hat{n}_i}, \tag{47}$$

where $\hat{n}_i$ is the normal to the surface S_i in global coordinates, and

$$A = -\frac{1}{2(2\pi)}\left(\frac{J_0 c}{A_0}\right)^2\int_{-\infty}^{\infty} e^{iq_z z}\chi_{yy}(q_z)dq_z, \tag{48}$$

$$B = -\frac{1}{2(2\pi)}\left(\frac{J_0 c}{A_0}\right)^2\int_{-\infty}^{\infty} e^{iq_z z}\chi_{zz}(q_z)dq_z, \tag{49}$$

$$D = -\frac{1}{2(2\pi)}\left(\frac{J_0 c}{A_0}\right)^2\int_{-\infty}^{\infty} e^{iq_z z}\chi_{yz}(q_z)dq_z, \tag{50}$$

where

$$\begin{aligned} \chi_{yy}(q_z) &= \frac{-\mu_B^2}{4\pi\hbar v_F}\text{Re}\left[\sqrt{1-x^2} + \frac{|q_z|}{2}\sin^{-1}\left(\sqrt{1-x^2}\right)\right], \\ \chi_{zz}(q_z) &= \frac{-\mu_B^2}{2\pi\hbar v_F}\left\{k_F + \frac{|q_z|}{2}\text{Re}\left[\sin^{-1}\left(\sqrt{1-x^2}\right)\right]\right\}, \\ \chi_{yz}(q_z) &= \frac{-i\mu_B^2 q_z}{8\pi\hbar v_F}\left[1 - \frac{1}{2}\text{Re}\left(\sqrt{1-x^2}\right)\right], \end{aligned} \tag{51}$$

and $x = 2k_F/q_z$. The integrals in Eqs. (48)-(50) are written in the global coordinates, where this is achieved by replacing $(y, q_y) \to (z, q_z)$ in Eq. (46). Notice that the integration over q_z in Eqs. (48)-(50) can be extended to $\pm\infty$, since all critical spanning vectors are much smaller than π/c within the range of Fermi energy $E_F < 0.2$eV considered in the low-energy effective theory for BiTeI surface states.

Unlike non-topological BiTeI, the magnetic interlayer exchange coupling, Eq. (47), mediated by the surface states of topological BiTeI allows for the coupling of

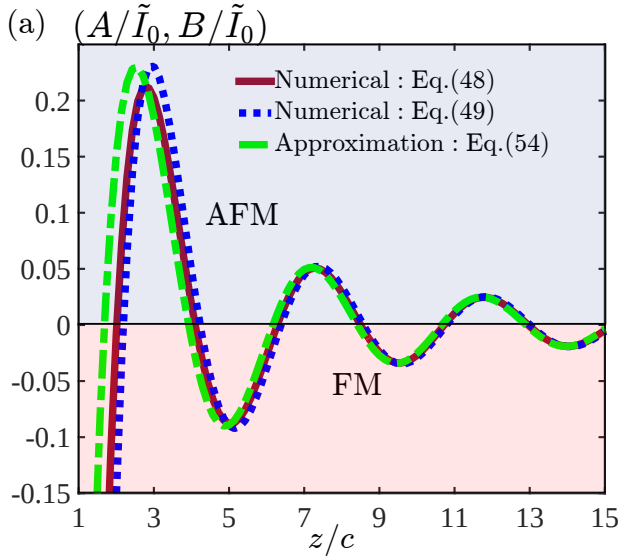

FIG. 9. Thickness dependence of amplitude for collinear parts of the interlayer exchange coupling per surface for (a) relatively thin samples of BiTeI and (b) thick samples of BiTeI. In (a) and (b) we take the parameter values $\hbar v_F = 1$ eVÅ and $E_F = 0.1$ eV. In both (a) and (b), the collinear exchange interaction oscillates with a period $\pi/k_F \approx 4.5c$ and decays as $z^{-3/2}$.

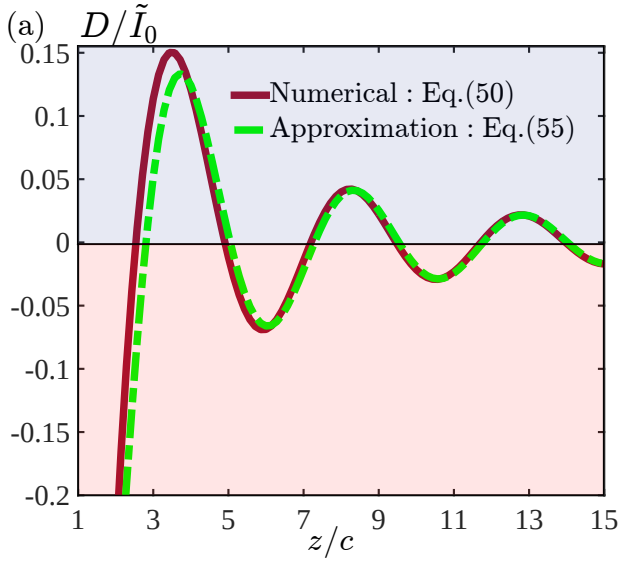

FIG. 10. Thickness dependence of amplitude for DM (non-collinear) part of the interlayer exchange coupling per surface for (a) relatively thin samples of BiTeI and (b) thick samples of BiTeI. In this figure we take the parameter values $\hbar v_F = 1$ eVÅ and $E_F = 0.1$ eV. In both (a) and (b), the DM interaction oscillates with a period $\pi/k_F \approx 4.5c$ and decays as $z^{-3/2}$.

collinear and non-collinear spins. The coupling between non-collinear spins is mediated by the DM interaction [74, 75] which in itself arises due to the spin-momentum coupling of the surface states. The appearance of the DM-mediated interlayer coupling is intertwined with the appearance of the topological phase of BiTeI, hence, the experimental measurements of such an interaction can be used as an indicator of a topological phase transition in this material.

Having found the general expression of the interlayer exchange coupling in the topological phase of BiTeI, Eq. (47), we proceed to determine its dependence on the sample thickness in the next section.

VII. SPATIAL DEPENDENCE OF EXCHANGE INTERACTION IN THE TOPOLOGICAL PHASE

In the trivial phase of BiTeI we have found that the interlayer exchange interaction for the system in Fig. 2(a)

decays with the thickness of BiTeI as z^{-2} for perpendicularly magnetized layers and z^{-1} for layers with magnetization parallel to the interface. In this section we investigate the change in this z dependence as BiTeI becomes a strong topological insulator.

The thickness dependence of the interlayer exchange coupling of topological BiTeI in Eq. (47) is numerically determined by the integrals in Eqs. (48)-(50). Due to the presence of a Kohn anomaly at $|q_z| = 2k_F$ the long-range behaviour of the interlayer exchange interaction between the magnetic chains, Fig. 8(b), can be obtained by integrating near the Kohn anomaly $q_z \in [2k_F - \epsilon, 2k_F + \epsilon]$ where $\epsilon \ll 2k_F$. Taking into account that $\chi_{zz,yy}(q_z) = \chi_{zz,yy}(-q_z)$ are even in q_z and $\chi_{yz}(q_z) = -\chi_{yz}(q_z)$ is odd in q_z, the integrals in Eqs. (48)-(50) close to the Kohn anomaly become

$$
\begin{aligned}
A &\approx \gamma\sqrt{k_F}\int_{2k_F-\epsilon}^{2k_F+\epsilon} \mathrm{Re}\left(\sqrt{q_z-2k_F}\right)\cos(q_z z)dq_z,\\
B &\approx \gamma\int_{2k_F-\epsilon}^{2k_F+\epsilon} \left[k_F+\sqrt{k_F}\mathrm{Re}\left(\sqrt{q_z-2k_F}\right)\right]\cos(q_z z)dq_z,\\
D &\approx \gamma\int_{2k_F-\epsilon}^{2k_F+\epsilon} \left[\sqrt{k_F}\mathrm{Re}\left(\sqrt{q_z-2k_F}\right)-2k_F\right]\sin(q_z z)dq_z,
\end{aligned}
\tag{52}
$$

where $\gamma = [(J_0\mu_B c)/(2\pi A_0\sqrt{\hbar v_F})]^2$. Recalling that the domain of the function $\mathrm{Re}(\sqrt{q_z-2k_F})$ is $q_z \geq 2k_F$, integrating Eq. (52) by parts once and then changing to the variable $q' = \sqrt{q_z - 2k_F}$, one obtains

$$
\begin{aligned}
A = B &\approx -\frac{\gamma\sqrt{k_F}}{z}\int_0^{\sqrt{\epsilon}} \sin(q'^2 z + 2k_F z)dq' \ ,\\
D &\approx \frac{\gamma\sqrt{k_F}}{z}\int_0^{\sqrt{\epsilon}} \cos(q'^2 z + 2k_F z)dq' \ .
\end{aligned}
\tag{53}
$$

Since the dominant contribution of the previous integral comes from $q' = 0$, we can extend its upper limit to $+\infty$ arriving at

$$
A = B \approx -\tilde{I}_0\left(\frac{c}{z}\right)^{3/2}\cos\left(2k_F z - \frac{\pi}{4}\right) \ , \tag{54}
$$

$$
D \approx -\tilde{I}_0\left(\frac{c}{z}\right)^{3/2}\sin\left(2k_F z - \frac{\pi}{4}\right) \ , \tag{55}
$$

where

$$
\tilde{I}_0 = \frac{\sqrt{k_F c\pi}}{2\hbar v_F}\left(\frac{J_0\mu_B}{2\pi A_0}\right)^2 \ . \tag{56}
$$

Then the interlayer exchange coupling between the magnetic chains for each surface is

$$
\begin{aligned}
I^i(z) = -\tilde{I}_0\left(\frac{c}{z}\right)^{3/2}&\left[\left(S_z^{\mathrm{T}}S_z^{\mathrm{B}} + S_{|\hat{n}_i|}^{\mathrm{T}}S_{|\hat{n}_i|}^{B}\right)\right.\\
&\left.\times\cos\left(2k_F z - \frac{\pi}{4}\right) + (\boldsymbol{S}^{\mathrm{T}}\times\boldsymbol{S}^{B})_{\hat{z}\times\hat{n}_i}\sin\left(2k_F z - \frac{\pi}{4}\right)\right].
\end{aligned}
\tag{57}
$$

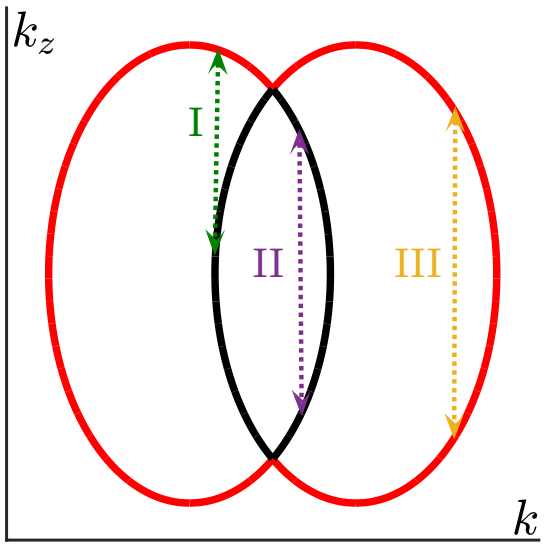

FIG. 11. Schematic representation of the types of electronic transitions along k_z through the Fermi surface: interband transitions between states with different helicities (I) and intraband transitions between states with the same helicities (II and III). Red (light) color indicates states with negative helicity and black (dark) color indicates states with positive helicity.

A comparison between the numerical calculation of the integrals Eqs. (48)-(50) with the analytical formulas in Eq. (54) in Figs. 9(a) and 10(a) reveals a close agreement for thicknesses $z/c < 5$. As the sample thickness exceed $z/c > 5$, the numerical and analytical results become essentially equal and overlap with each other as shown in Figs. 9(b) and 10(b). The interlayer exchange interaction mediated by the different surface states is characterized by a single period of oscillation, π/k_F, and the envelope of these oscillations decays with the thickness of the sample as $z^{-3/2}$.

We have seen that the magnetic exchange of the system in Fig. 2(a) for topological BiTeI reduces to the exchange between the magnetic chains at the edges of the sample and it is mediated by the surface states, Fig. 8(b). Unlike the trivial phase of BiTeI, the magnetic interlayer exchange interaction per surface in topological BiTeI couples both collinear and non-collinear spins due to the appearance of the DM interaction, and it decays with the thickness of BiTeI as $z^{-3/2}$.

VIII. DISCUSSION

In this section, we start by first highlighting the physical differences of the interlayer exchange interaction mediated by BiTeI in its trivial and topological phases. In the trivial phase of BiTeI, we have found that the interlayer RKKY interaction is collinear and anisotropic for spin alignment between the out-of-plane and in-plane directions. This can be understood from a clear picture

Matrix Element (x, y, z)	Interband $(\nu = -\mu)$	Intraband $(\nu = \mu)$
$\langle \mu, k_z', \boldsymbol{k}_\parallel \vert \sigma_x \vert \boldsymbol{k}_\parallel, k_z, \nu \rangle$	$i\mu e^{iq_z z}\cos(\phi_k)$	$\mu e^{iq_z z}\sin(\phi_k)$
$\langle \mu, k_z', \boldsymbol{k}_\parallel \vert \sigma_y \vert \boldsymbol{k}_\parallel, k_z, \nu \rangle$	$i\mu e^{iq_z z}\sin(\phi_k)$	$-\mu e^{iq_z z}\cos(\phi_k)$
$\langle \mu, k_z', \boldsymbol{k}_\parallel \vert \sigma_z \vert \boldsymbol{k}_\parallel, k_z, \nu \rangle$	$\mu e^{iq_z z}$	0

TABLE II. Matrix elements of the $\boldsymbol{k}_\parallel$-preserving interband and intraband transitions along k_z due to interaction with a ferromagnetic layer with magnetization in the x, y or z-directions. Here, $q_z = k_z - k_z'$ and $|\boldsymbol{k}, \mu\rangle$ are given by Eq. (2).

of the underlying physical processes contributing to the interlayer RKKY interaction, which are $\boldsymbol{k}_\parallel$-preserving interband and intraband transitions along k_z through the Fermi surface (Fig. 11). For an electron undergoing an interband transition between bands with different helicities, the requirement of in-plane momentum conservation means that its spin must flip (shown as process I in Fig. 11). This spin flip can be achieved through interacting with a ferromagnetic layer magnetized either in the out-of plane or in-plane directions, since the corresponding matrix elements are all nonvanishing, as shown in Table II. On the other hand, an electron's spin is preserved for intraband transitions (shown as processes II and III in Fig. 11). This is only possible via interacting with a ferromagnetic layer with an in-plane magnetization, since the matrix element corresponding to the interaction with a z-polarized ferromagnet is zero, as shown in Table II. It follows from Table II that the interlayer exchange interaction is collinear with vanishing interaction between magnetizations along different directions, because the product of any two different matrix elements within the same type of transitions averages out to zero over all directions [76]. Futhermore, since the interlayer exchange coupling between layers with out-of-plane magnetizations I_{zz} is contributed only by interband transitions, it is different from that between layers with in-plane magnetizations $I_{xx,yy}$ that is contributed by both interband and intraband transitions. The asymptotic behavior of the two cases are distinguished by their distinct power laws going as z^{-2} and z^{-1} respectively at large thicknesses.

In the topological phase of BiTeI, we have shown that the interlayer exchange interaction becomes limited to the magnetic chains residing at the edges of the sample and it is mediated via the spin-momentum-locked surface states. Unlike the trivial phase of BiTeI, surface helical electrons in the topological phase mediate the RKKY interaction and due to their SOC they allow for magnetic exchange between non-collinear spins arising from the DM interaction. In general, the collinear and DM contributions of the exchange coupling on each surface oscillate with a single period determined by the Fermi wavelength and decay with the thickness of BiTeI as $z^{-3/2}$. The DM term is present on each surface but the sign of its coupling is dependent on the surface orientation (*e.g.*, it has opposite signs on opposite surfaces) while the collinear terms carry the same sign for all surfaces.

We now discuss how the main features of the interlayer exchange interaction in the trivial and topological phases may allow for the experimental detection of the topological phase transition via the measurement of this interaction. Two setups can be devised for the detection of the topological phase transition in BiTeI. First, using ferromagnets with orthogonal magnetizations, the collinear exchange terms will vanish in the topological phase and the exchange is contributed only by the non-collinear DM terms from each surface. Since the non-collinear terms are absent in the trivial phase, the interlayer exchange coupling for this setup will be zero when the pressure is below the critical pressure for topological phase transition. Beyond this pressure, the interlayer exchange coupling will be dominated by the surface DM terms. As noted in Eq. (57), the DM term has opposite signs for surfaces with opposite normal vectors $\hat{n}_i$, and all the DM contributions will cancel from pairs of opposite surfaces in a BiTeI sample with an even number of perfectly aligned side surfaces. Therefore, experimental detection of a non-vanishing interlayer exchange coupling in the topological phase requires a sample with an odd number of side surfaces (*e.g.*, a pentagonal prism) or irregular side surfaces with minimum cancellation of DM coupling from opposite surfaces. Another possibility is to avoid cancellation from opposite surfaces altogether by localizing the measurement geometry on only one side surface.

Second, using ferromagnets with parallel magnetizations, the DM part of the exchange will vanish in the topological phase and the exchange interaction is contributed only by collinear terms in both phases. Even though both phases are characterized by collinear exchange terms, there is a distinct dependence of the exchange on the thickness, z^{-1} (z^{-2}) for magnetization parallel (orthogonal) to the interface in the trivial phase and $z^{-3/2}$ in the topological phase, and the change of this thickness dependence can serve as an indicator for the topological phase transition, with the advantage that this measurement scheme does not rely on the number of surfaces simultaneously measured.

Experimentally, the interlayer exchange coupling in heterostructures composed of magnetic and non-magnetic materials can be determined by the magneto-optical Kerr effect, magneto-resistance oscillations, polarized neutron reflectrometry and ferromagnetic resonance experiments [27, 28, 47, 48, 77–84]. In the trivial phase of BiTeI the observation of the phenomena described in our work requires a quantitative determination of the interlayer exchange coupling for both ferromagnetically and anti-ferromagnetically coupled systems, together with the ability to discern the in-plane and out-of-plane components of the coupling. To this end, we suggest that experiments relying on ferromagnetic resonances would be a suitable platform for this observation [81–84]. The detection of the interlayer exchange coupling in the topological phase and the topological phase transition requires pressure-controlled mea-

surements of magneto-resistance, spin susceptibility or ferromagnetic resonances. These methods have been previously utilized to study the pressure effects on the interlayer exchange coupling in Fr/Cr multilayers [85], 2D ferromagnets [86] and FeCoB/Ru/FeCoB heterostructures [87]. These well-established experimental methods coupled with the controlled growth of bulk Rashba semiconductors [8–12] should make the observation of the unconventional interlayer exchange interaction mediated by these exotic materials readily accessible.

IX. CONCLUSIONS

We have presented a theory for the interlayer exchange coupling between two ferromagnets deposited on opposite surfaces of the bulk Rashba semiconductor BiTeI, in its non-topological and topological phases. Our work highlights the unconventional dependence of the exchange interaction on the BiTeI spacer's topological phase and thickness, as well as the ferromagnets' spin orientations.

In the non-topological phase of BiTeI, our calculation of the interlayer exchange coupling revealed that the latter only couples collinear spins and is strongly dependent on the magnetization direction of the ferromagnets. If the ferromagnets are deposited on opposite surfaces along the stacking direction of BiTeI and have an out-of-plane magnetization direction, then the interlayer exchange coupling behaves in a qualitatively similar way to that in a metallic spacer with an ellipsoidal Fermi surface. The interlayer exchange coupling shows a single period of oscillation and decays with the thickness of the spacer z as z^{-2}, and the only effect introduced by the Rashba SOC is the renormalization of the amplitude of the exchange interaction. However, if the ferromagnets have an in-plane magnetization direction, the interlayer exchange interaction exhibits significant qualitative differences compared to a spin-degenerate metal. The exchange interaction displays two periods of spatial oscillations and decays as z^{-1} with an amplitude that is proportional to α^2 (where α is the strength of the Rashba SOC) due to the interplay between the Rashba SOC and interfacing spins.

In the topological phase of BiTeI, only the surface states can mediate the interlayer exchange interaction resulting in a coupling between the one-dimensional spin chains at the edges of the two ferromagnets. In addition to collinear spins coupling, coupling of non-collinear spins emerges due to the presence of DM interaction, and both are characterized by a single oscillation period given by the Fermi wavelength and decay with the thickness of BiTeI as $z^{-3/2}$. The qualitative differences in the interlayer exchange coupling of BiTeI between the trivial and topological phases can be used as a signature to detect the topological phase transition in this exotic material. The theory and findings we obtained for the topological phase of BiTeI are also applicable to other strong topological insulators such as Bi_2Se_3 and Bi_2Te_3.

ACKNOWLEDGMENTS

We thank Tim Mewes for fruitful discussions. This work was supported by the U.S. Department of Energy, Office of Science, Basic Energy Sciences under Early Career Award #DE-SC0019326.

Appendix A: Spin Susceptibility of Spin-Orbit-Coupled Systems

In this section we provide a derivation of the non-interacting spin susceptibility of a spin-orbit-coupled electron gas from the Matsubara Green's function formalism. The spin susceptibility can be written as

$$\chi_{ab}(\boldsymbol{q}, iq_n) = -\mu_B^2 \frac{1}{\beta} \sum_{ik_n} \sum_{\boldsymbol{k}} \mathrm{Tr}\left\{ G_{\boldsymbol{k}}(ik_n)\sigma_a \times G_{\boldsymbol{k}+\boldsymbol{q}}(ik_n + q_n)\sigma_b \right\} , \quad \text{(A1)}$$

where $\beta = 1/(k_B T)$, k_B is the Boltzmann constant and T is the temperature, k_n and q_n are the fermionic Matsubara frequencies, and Tr denotes a trace. The Matsubara Green's function $G_{\boldsymbol{k}}(ik_n)$ is

$$G_{\boldsymbol{k}}(ik_n) = \sum_{\mu=\pm} \frac{|\boldsymbol{k}, \mu\rangle\langle\mu, \boldsymbol{k}|}{ik_n - E_{\boldsymbol{k},\mu}} , \quad \text{(A2)}$$

where $\mu = \pm$ denotes the band index and $|\boldsymbol{k}, \mu\rangle$ the spinor wavefunction of the μ^{th}-band energy eigenstate. Substituting Eq. (A2) into Eq. (A1) yields

$$\chi_{ab}(\boldsymbol{q}, iq_n) = -\mu_B^2 \frac{1}{\beta} \sum_{ik_n} \sum_{\boldsymbol{k}} \sum_{\mu,\nu} \mathrm{Tr}\left\{ \frac{|\boldsymbol{k}, \mu\rangle\langle\mu, \boldsymbol{k}|}{ik_n - E_{\boldsymbol{k},\mu}}\sigma_a \times \frac{|\boldsymbol{k}+\boldsymbol{q}, \nu\rangle\langle\nu, \boldsymbol{k}+\boldsymbol{q}|}{ik_n + iq_n - E_{\boldsymbol{k}+\boldsymbol{q},\nu}}\sigma_b \right\} . \quad \text{(A3)}$$

Invariance of the trace under cyclic permutations leads to

$$\chi_{ab}(\boldsymbol{q}, iq_n) = -\mu_B^2 \frac{1}{\beta} \sum_{ik_n} \sum_{\boldsymbol{k}} \sum_{\mu,\nu} \left[\frac{\langle\mu, \boldsymbol{k}|\sigma_a|\boldsymbol{k}+\boldsymbol{q}, \nu\rangle\langle\nu, \boldsymbol{k}+\boldsymbol{q}|\sigma_b|\boldsymbol{k}, \mu\rangle}{(ik_n - E_{\boldsymbol{k},\mu})(ik_n + iq_n - E_{\boldsymbol{k}+\boldsymbol{q},\nu})} \right] . \quad \text{(A4)}$$

Performing the Matsubara sum, the above reduces to

$$\chi_{ab}(\boldsymbol{q}, iq_n) = -\mu_B^2 \sum_{\boldsymbol{k}} \sum_{\mu,\nu} \frac{f(E_{\boldsymbol{k},\mu}) - f(E_{\boldsymbol{k}+\boldsymbol{q},\nu})}{iq_n + E_{\boldsymbol{k},\mu} - E_{\boldsymbol{k}+\boldsymbol{q},\nu}} \times \mathcal{F}_{ab}^{\mu\nu}(\boldsymbol{k}, \boldsymbol{k}+\boldsymbol{q}) . \quad \text{(A5)}$$

where $f(E_{\boldsymbol{k},\mu})$ is the Fermi function, and $\mathcal{F}_{ab}^{\mu\nu}(\boldsymbol{k}, \boldsymbol{k}+\boldsymbol{q}) = \langle\mu, \boldsymbol{k}|\sigma_a|\boldsymbol{k}+\boldsymbol{q}, \nu\rangle\langle\nu, \boldsymbol{k}+\boldsymbol{q}|\sigma_b|\boldsymbol{k}, \mu\rangle$ is a form factor. Analytically continuing to the real frequency $iq_n \to \omega + i\delta$

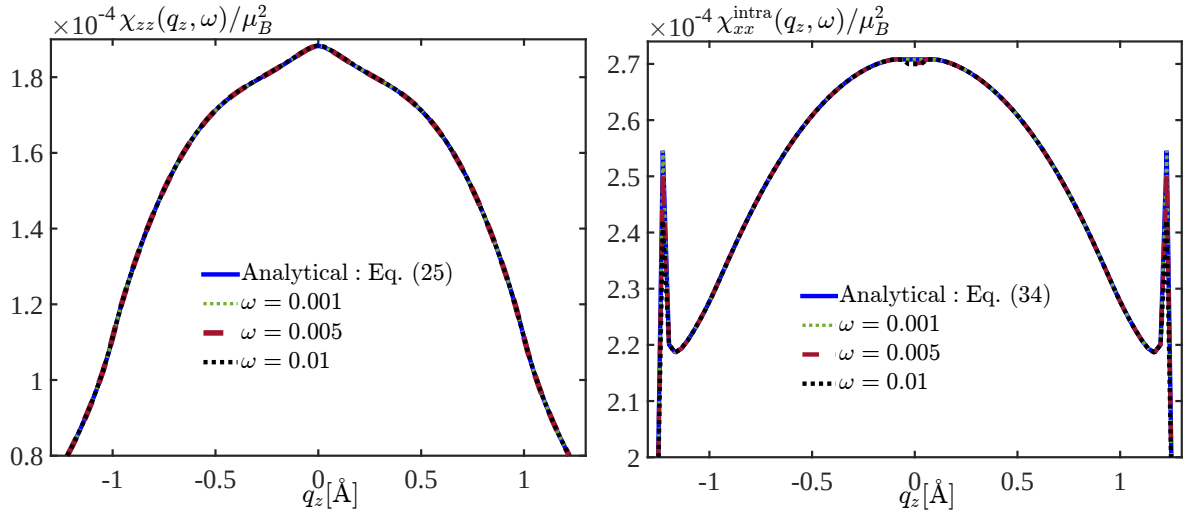

FIG. 12. Comparison of $\lim_{\omega\to 0}\chi^{\mu\nu}_{ss'}(\boldsymbol{q},\omega)$ to the analytical expressions in Eq. (22) (left panel) and (30) (right panel). In both panels we can notice the equivalence of $\lim_{\omega\to 0}\chi^{\mu\nu}_{ss'}(\boldsymbol{q},\omega)$ and the analytical forms.

($\delta = 0^+$), one obtains the final expression of the retarded spin susceptibility

$$\chi_{ab}(\boldsymbol{q},\omega) = -\mu_B^2 \sum_{\boldsymbol{k}}\sum_{\mu,\nu} \frac{f(E_{\boldsymbol{k},\mu}) - f(E_{\boldsymbol{k}+\boldsymbol{q},\nu})}{E_{\boldsymbol{k},\mu} - E_{\boldsymbol{k}+\boldsymbol{q},\nu} + \omega + i\delta} \times \mathcal{F}^{\mu\nu}_{ab}(\boldsymbol{k},\boldsymbol{k}+\boldsymbol{q}). \tag{A6}$$

Eq. (A6) in its static limit, $\omega \to 0$, reduces to Eq. (9) for three dimensions and $\boldsymbol{q}_\parallel = 0$, and for two dimensions it reduces to Eq. (43) in the main text.

Appendix B: Static Spin Susceptibility of Bulk Rashba Semiconductors

In this appendix we discuss the static limit of the spin susceptibility in a bulk Rashba semiconductor. Here we start with the dynamic spin susceptibility, *i.e.*,

$$\chi^{\mu\nu}_{ab}(\boldsymbol{q},\omega) = -\mu_B^2 \int \frac{d^3\boldsymbol{k}}{(2\pi)^3} \times \frac{f(E_{\boldsymbol{k},\mu}) - f(E_{\boldsymbol{k}+\boldsymbol{q},\nu})}{E_{\boldsymbol{k},\mu} - E_{\boldsymbol{k}+\boldsymbol{q},\nu} + \omega + i\delta} \mathcal{F}^{\mu\nu}_{ab}(\boldsymbol{k},\boldsymbol{k}+\boldsymbol{q}). \tag{B1}$$

The real part of the spin susceptibility is

$$\chi^{\mu\nu}_{ab}(\boldsymbol{q},\omega) = -\mu_B^2 \mathcal{P}\int \frac{d^3\boldsymbol{k}}{(2\pi)^3} \times \frac{f(E_{\boldsymbol{k},\mu}) - f(E_{\boldsymbol{k}+\boldsymbol{q},\nu})}{E_{\boldsymbol{k},\mu} - E_{\boldsymbol{k}+\boldsymbol{q},\nu} + \omega} \mathcal{F}^{\mu\nu}_{ab}(\boldsymbol{k},\boldsymbol{k}+\boldsymbol{q}), \tag{B2}$$

where $\mathcal{P}$ denotes the principal value of the integral. The latter integral, in its most general form, has contribution from complex and real poles, and in order to correctly account for these contributions in the static limit, one needs to consider $\lim_{\omega\to 0}\chi^{\mu\nu}_{ss'}(\boldsymbol{q},\omega)$. However, we have two distinct cases that can be treated differently. First: the case in which the complex poles have vanishing contributions as $\omega \to 0$. In this case, we can directly take $\omega \to 0$ in the integral in Eq. (B2), such that

$$\chi^{\mu\nu}_{ab}(\boldsymbol{q},0) = \mu_B^2 \mathcal{P}\int \frac{d^3\boldsymbol{k}}{(2\pi)^3} \times \frac{f(E_{\boldsymbol{k},\mu}) - f(E_{\boldsymbol{k}+\boldsymbol{q},\nu})}{E_{\boldsymbol{k}+\boldsymbol{q},\nu} - E_{\boldsymbol{k},\mu}} \mathcal{F}^{\mu\nu}_{ab}(\boldsymbol{k},\boldsymbol{k}+\boldsymbol{q}), \tag{B3}$$

An example of such a case is the 3D electron gas [29]. Second: the case in which the complex poles of the integral in Eq. (B2) have non-vanishing contributions as $\omega \to 0$. In this case taking $\omega \to 0$ in Eq. (B2) leads to unphysical results. Instead, one needs to find $\lim_{\omega\to 0}\chi^{\mu\nu}_{ss'}(\boldsymbol{q},\omega)$ to correctly account for the contribution from all poles. This scenario is displayed in the Rashba SOC metal in 2D [88].

For a bulk Rashba semiconductor, even though it may seem similar to the 2D Rashba SOC metal, we find that for $(q_x, q_y) = (0, 0)$ the contributions of the complex poles vanish as $\omega \to 0$ because of the additional k_z dependence, and that the static spin susceptibility is given by Eq. (10). We have numerically verified the equivalence of our analytical forms of the static spin susceptibility, Eqs. (22) and (30), and $\lim_{\omega\to 0}\chi^{\mu\nu}_{ss'}(\boldsymbol{q},\omega)$, as shown in Fig. 12.

[1] J. Nitta, T. Akazaki, H. Takayanagi, and T. Enoki, Phys. Rev. Lett. **78**, 1335 (1997).
[2] C. R. Ast, J. Henk, A. Ernst, L. Moreschini, M. C. Falub, D. Pacilé, P. Bruno, K. Kern, and M. Grioni, Phys. Rev. Lett. **98**, 186807 (2007).
[3] S. LaShell, B. A. McDougall, and E. Jensen, Phys. Rev. Lett. **77**, 3419 (1996).
[4] I. Gierz, T. Suzuki, E. Frantzeskakis, S. Pons, S. Ostanin, A. Ernst, J. Henk, M. Grioni, K. Kern, and C. R. Ast, Phys. Rev. Lett. **103**, 046803 (2009).
[5] Y. M. Koroteev, G. Bihlmayer, J. E. Gayone, E. V. Chulkov, S. Blügel, P. M. Echenique, and P. Hofmann, Phys. Rev. Lett. **93**, 046403 (2004).
[6] A. F. Santander-Syro, F. Fortuna, C. Bareille, T. C. Rödel, G. Landolt, N. C. Plumb, J. H. Dil, and M. Radovic, Nature Materials **13**, 1085 (2014).
[7] Y. A. Bychkov and E. I. Rashba, JETP Lett. **39**, 78 (1984).
[8] M. S. Bahramy and N. Ogawa, Advanced Materials **29**, 10.1002/adma.201605911 (2017).
[9] K. Ishizaka, M. S. Bahramy, H. Murakawa, M. Sakano, T. Shimojima, T. Sonobe, K. Koizumi, S. Shin, H. Miyahara, A. Kimura, K. Miyamoto, T. Okuda, H. Namatame, M. Taniguchi, R. Arita, N. Nagaosa, K. Kobayashi, Y. Murakami, R. Kumai, Y. Kaneko, and Y. Onose, Nature Materials **10**, 521 (2011).
[10] H. Murakawa, M. S. Bahramy, M. Tokunaga, Y. Kohama, C. Bell, Y. Kaneko, N. Nagaosa, H. Y. Hwang, and Y. Tokura, Science **342**, 1490 (2013).
[11] M. Kanou and T. Sasagawa, Journal of Physics: Condensed Matter **25**, 135801 (2013).
[12] B. Fülöp, Z. Tajkov, J. Pető, P. Kun, J. Koltai, L. Oroszlány, E. Tóvári, H. Murakawa, Y. Tokura, S. Bordács, L. Tapasztó, and S. Csonka, 2D Materials **5**, 031013 (2018).
[13] M. S. Bahramy, R. Arita, and N. Nagaosa, Phys. Rev. B **84**, 041202 (2011).
[14] M. S. Bahramy, B. Yang, R. Arita, and N. Nagaosa, Nature Communications **3**, 677 (2012).
[15] Y. Qi, W. Shi, P. G. Naumov, N. Kumar, R. Sankar, W. Schnelle, C. Shekhar, F.-C. Chou, C. Felser, B. Yan, and S. A. Medvedev, Advanced Materials **29**, 1605965 (2017).
[16] X. Xi, C. Ma, Z. Liu, Z. Chen, W. Ku, H. Berger, C. Martin, D. B. Tanner, and G. L. Carr, Phys. Rev. Lett. **111**, 155701 (2013).
[17] D. VanGennep, A. Linscheid, D. E. Jackson, S. T. Weir, Y. K. Vohra, H. Berger, G. R. Stewart, R. G. Hennig, P. J. Hirschfeld, and J. J. Hamlin, Journal of Physics: Condensed Matter **29**, 09LT02 (2017).
[18] M. K. Tran, J. Levallois, P. Lerch, J. Teyssier, A. B. Kuzmenko, G. Autès, O. V. Yazyev, A. Ubaldini, E. Giannini, D. van der Marel, and A. Akrap, Phys. Rev. Lett. **112**, 047402 (2014).
[19] J. I. Facio, D. Efremov, K. Koepernik, J.-S. You, I. Sodemann, and J. van den Brink, Phys. Rev. Lett. **121**, 246403 (2018).
[20] J. Liu and D. Vanderbilt, Phys. Rev. B **90**, 155316 (2014).
[21] I. P. Rusinov, T. V. Menshchikova, I. Y. Sklyadneva, R. Heid, K.-P. Bohnen, and E. V. Chulkov, New Journal of Physics **18**, 113003 (2016).
[22] V. K. Joshi, Engineering Science and Technology, an International Journal **19**, 1503 (2016).
[23] I. Žutić, J. Fabian, and S. Das Sarma, Rev. Mod. Phys. **76**, 323 (2004).
[24] M. Z. Hasan and C. L. Kane, Rev. Mod. Phys. **82**, 3045 (2010).
[25] X.-L. Qi and S.-C. Zhang, Rev. Mod. Phys. **83**, 1057 (2011).
[26] B. A. Bernevig and T. L. Hughes, *Topological Insulators and Topological Superconductors* (Princeton University Press, New York, 2013).
[27] P. Grünberg, R. Schreiber, Y. Pang, M. B. Brodsky, and H. Sowers, Phys. Rev. Lett. **57**, 2442 (1986).
[28] M. N. Baibich, J. M. Broto, A. Fert, F. N. Van Dau, F. Petroff, P. Etienne, G. Creuzet, A. Friederich, and J. Chazelas, Phys. Rev. Lett. **61**, 2472 (1988).
[29] M. A. Ruderman and C. Kittel, Phys. Rev. **96**, 99 (1954).
[30] T. Kasuya, Progress of Theoretical Physics **16**, 45 (1956).
[31] K. Yosida, Phys. Rev. **106**, 893 (1957).
[32] A. M. Black-Schaffer, Phys. Rev. B **81**, 205416 (2010).
[33] H. Hatami, T. Kernreiter, and U. Zülicke, Phys. Rev. B **90**, 045412 (2014).
[34] D. Mastrogiuseppe, N. Sandler, and S. E. Ulloa, Phys. Rev. B **90**, 161403 (2014).
[35] D. Mastrogiuseppe, N. Sandler, and S. E. Ulloa, Phys. Rev. B **93**, 094433 (2016).
[36] H.-R. Chang, J. Zhou, S.-X. Wang, W.-Y. Shan, and D. Xiao, Phys. Rev. B **92**, 241103 (2015).
[37] P. Bruno and C. Chappert, Phys. Rev. Lett. **67**, 1602 (1991).
[38] P. Bruno and C. Chappert, Phys. Rev. B **46**, 261 (1992).
[39] M. Stiles, Interlayer exchange coupling, in *Ultrathin Magnetic Structures III: Fundamentals of Nanomagnetism*, edited by J. A. C. Bland and B. Heinrich (Springer Berlin Heidelberg, Berlin, Heidelberg, 2005) pp. 99–142.
[40] V. Mourik, K. Zuo, S. M. Frolov, S. R. Plissard, E. P. A. M. Bakkers, and L. P. Kouwenhoven, Science **336**, 1003 (2012).
[41] S.-G. Je, D.-H. Kim, S.-C. Yoo, B.-C. Min, K.-J. Lee, and S.-B. Choe, Phys. Rev. B **88**, 214401 (2013).
[42] G. Finocchio, F. Büttner, R. Tomasello, M. Carpentieri, and M. Kläui, Journal of Physics D: Applied Physics **49**, 423001 (2016).
[43] L. Ye, J. G. Checkelsky, F. Kagawa, and Y. Tokura, Phys. Rev. B **91**, 201104 (2015).
[44] J. S. Lee, G. A. H. Schober, M. S. Bahramy, H. Murakawa, Y. Onose, R. Arita, N. Nagaosa, and Y. Tokura, Phys. Rev. Lett. **107**, 117401 (2011).
[45] C. Bell, M. S. Bahramy, H. Murakawa, J. G. Checkelsky, R. Arita, Y. Kaneko, Y. Onose, M. Tokunaga, Y. Kohama, N. Nagaosa, Y. Tokura, and H. Y. Hwang, Phys. Rev. B **87**, 081109 (2013).
[46] W. Kohn, Phys. Rev. Lett. **2**, 393 (1959).
[47] J. Unguris, R. J. Celotta, and D. T. Pierce, Phys. Rev. Lett. **67**, 140 (1991).
[48] S. T. Purcell, W. Folkerts, M. T. Johnson, N. W. E. McGee, K. Jager, J. aan de Stegge, W. B. Zeper, W. Hoving, and P. Grünberg, Phys. Rev. Lett. **67**, 903 (1991).
[49] Y. Yafet, Phys. Rev. B **36**, 3948 (1987).
[50] J. H. Van Vleck, Phys. Rev. **29**, 727 (1927).
[51] J. H. Van Vleck, Phys. Rev. **30**, 31 (1927).

[52] J. H. Van Vleck, Phys. Rev. **31**, 587 (1928).
[53] J. Zhou, W.-Y. Shan, and D. Xiao, Phys. Rev. B **91**, 241302 (2015).
[54] S. K. Yip, Phys. Rev. B **65**, 144508 (2002).
[55] C. Kittel, *Indirect Exchange Interactions in Metals*, edited by F. Seitz, D. Turnbull, and H. Ehrenreich, Solid State Physics, Vol. 22 (Academic Press, New York, 1969) pp. 1 – 26.
[56] The exchange between two magnetic chains at the edge of a 2D conventional metal is found, in the continuum limit, by integrating the magnetic exchange between two single impurities ($J(\boldsymbol{r}) \propto \sin(2k_F r)/r^2$ where r is the distance between the impurities [55]) over the length of the these chains. This leads to an interlayer exchange that decays with the distance between the chains z as $1/z$.
[57] C.-X. Liu, B. Roy, and J. D. Sau, Phys. Rev. B **94**, 235421 (2016).
[58] I. Garate and M. Franz, Phys. Rev. B **81**, 172408 (2010).
[59] J.-J. Zhu, D.-X. Yao, S.-C. Zhang, and K. Chang, Phys. Rev. Lett. **106**, 097201 (2011).
[60] D. A. Abanin and D. A. Pesin, Phys. Rev. Lett. **106**, 136802 (2011).
[61] D. K. Efimkin and V. Galitski, Phys. Rev. B **89**, 115431 (2014).
[62] D. Culcer, Phys. Rev. B **84**, 235411 (2011).
[63] C. S. Ho and M. B. A. Jalil, AIP Advances **7**, 055926 (2017).
[64] A. A. Zyuzin and D. Loss, Phys. Rev. B **90**, 125443 (2014).
[65] M. Shiranzaei, H. Cheraghchi, and F. Parhizgar, Phys. Rev. B **96**, 024413 (2017).
[66] F. Zhang, C. L. Kane, and E. J. Mele, Phys. Rev. B **86**, 081303 (2012).
[67] R.-L. Chu, J. Shi, and S.-Q. Shen, Phys. Rev. B **84**, 085312 (2011).
[68] Y. Zhang, Y. Ran, and A. Vishwanath, Phys. Rev. B **79**, 245331 (2009).
[69] C. L. Kane and E. J. Mele, Phys. Rev. Lett. **95**, 146802 (2005).
[70] L. Fu, Phys. Rev. Lett. **103**, 266801 (2009).
[71] W.-M. Huang, C.-H. Chang, and H.-H. Lin, Phys. Rev. B **73**, 241307 (2006).
[72] T. Ando, Journal of the Physical Society of Japan **75**, 074716 (2006).
[73] E. H. Hwang and S. Das Sarma, Phys. Rev. B **75**, 205418 (2007).
[74] I. Dzyaloshinsky, Journal of Physics and Chemistry of Solids **4**, 241 (1958).
[75] T. Moriya, Phys. Rev. **120**, 91 (1960).
[76] In the case of two isolated magnetic impurities placed along the c-axis of bulk Rashba semiconductors, the DM interaction is found to vanish [89], consistent with our finding.
[77] W. R. Bennett, W. Schwarzacher, and W. F. Egelhoff, Phys. Rev. Lett. **65**, 3169 (1990).
[78] S. S. P. Parkin, N. More, and K. P. Roche, Phys. Rev. Lett. **64**, 2304 (1990).
[79] M. Lang, M. Montazeri, M. C. Onbasli, X. Kou, Y. Fan, P. Upadhyaya, K. Yao, F. Liu, Y. Jiang, W. Jiang, K. L. Wong, G. Yu, J. Tang, T. Nie, L. He, R. N. Schwartz, Y. Wang, C. A. Ross, and K. L. Wang, Nano Letters **14**, 3459 (2014).
[80] S. R. Spurgeon, J. D. Sloppy, D. M. D. Kepaptsoglou, P. V. Balachandran, S. Nejati, J. Karthik, A. R. Damodaran, C. L. Johnson, H. Ambaye, R. Goyette, V. Lauter, Q. M. Ramasse, J. C. Idrobo, K. K. S. Lau, S. E. Lofland, J. M. Rondinelli, L. W. Martin, and M. L. Taheri, ACS Nano **8**, 894 (2014).
[81] B. Khodadadi, J. B. Mohammadi, J. M. Jones, A. Srivastava, C. Mewes, T. Mewes, and C. Kaiser, Phys. Rev. Applied **8**, 014024 (2017).
[82] Y. Cui, B. Khodadadi, S. Schäfer, T. Mewes, J. Lu, and S. A. Wolf, Applied Physics Letters **102**, 162403 (2013).
[83] S. Klingler, A. Chumak, T. Mewes, B. Khodadadi, C. Mewes, C. Dubs, O. Surzhenko, B. Hillebrands, and A. Conca, Journal of Physics D: Applied Physics **48**, 015001 (2015).
[84] Z. Zhang, L. Zhou, P. E. Wigen, and K. Ounadjela, Phys. Rev. Lett. **73**, 336 (1994).
[85] K. Suenaga, S. Higashihara, M. Ohashi, G. Oomi, M. Hedo, Y. Uwatoko, K. Saito, S. Mitani, and K. Takanashi, Phys. Rev. Lett. **98**, 207202 (2007).
[86] H. Manaka, I. Yamada, M. Nishi, and T. Goto, Journal of the Physical Society of Japan **70**, 1390 (2001).
[87] S. Li, G.-X. Miao, D. Cao, Q. Li, J. Xu, Z. Wen, Y. Dai, S. Yan, and Y. Lü, ACS Applied Materials & Interfaces **10**, 8853 (2018).
[88] M. Pletyukhov and V. Gritsev, Phys. Rev. B **74**, 045307 (2006).
[89] S.-X. Wang, H.-R. Chang, and J. Zhou, Phys. Rev. B **96**, 115204 (2017).